



Wintertime hygroscopic growth factors (HGFs) of accumulation mode particles and their linkage to chemical composition in a heavily polluted urban atmosphere of Kanpur at the Centre of IGP, India: Impact of ambient relative humidity

Anil Kumar Mandariya ^a, S.N. Tripathi ^{a,b,*}, Tarun Gupta ^{a,b}, Gaurav Mishra ^c

^a Department of Civil Engineering, Indian Institute of Technology, Kanpur, India

^b Centre for Environmental Science and Engineering, CESE, IIT Kanpur, India

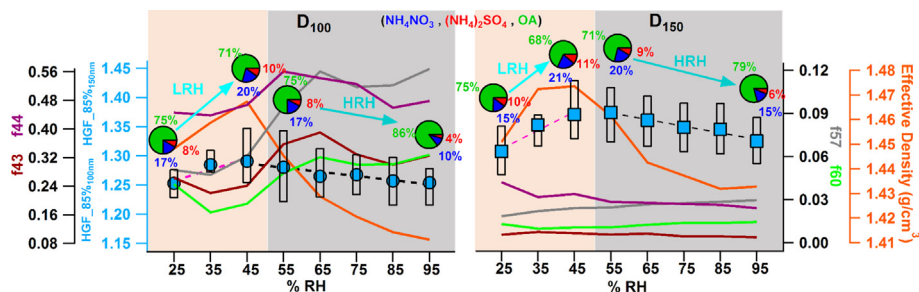
^c Nuclear Engineering and Technology Programme, Department of Mechanical Engineering, IIT Kanpur, India



HIGHLIGHTS

- HGF of accumulation mode aerosols at 85% RH reported the first time from India.
- Mean HGF_{85%}_{100nm} and HGF_{85%}_{150nm} were 1.27 ± 0.06 and 1.34 ± 0.07 , respectively.
- Mean HGF_{85%} reflected two distinct variations at LRH $\leq 50\%$ and HRH $> 50\%$.
- At LRH, HGF_{85%} correlated linearly (positive) with f44 and effective density.
- HGF_{85%} correlated linearly (inverse) with f44 and effective density at HRH.

GRAPHICAL ABSTRACT



ARTICLE INFO

Article history:

Received 30 August 2019

Received in revised form 14 October 2019

Accepted 1 November 2019

Available online 23 November 2019

Editor: Pingqiang Fu

Keywords:

H-TDMA

HGF_{85%}

Accumulation mode aerosol particles

OA

f44

HRH

LRH

ABSTRACT

This study reported results of the wintertime simultaneous measurements of hygroscopic growth factors (HGFs) and particle-phase chemical composition of accumulation mode particles using a self-assembled Hygroscopic Tandem Differential Mobility Analyzer (H-TDMA) and an Aerodyne High-Resolution Time-of-Flight Aerosol Mass Spectrometer (HR-ToF-AMS), respectively at a heavily polluted urban atmosphere of Kanpur, situated in the center of IGP in India. HGFs at 85% relative humidity (RH) and the size-resolved composition of ambient aerosol particles (dry electrical mobility diameters of 100 and 150 nm) were investigated. HGF_{85%} was found to increase with particle size. The relative mass fraction of organic aerosol (OA) and NH_4NO_3 are probably the major contributors to the fluctuation of the HGF_{85%} for both particle sizes. The HGF_{85%} of accumulation mode particles were observed to increase from the minimum value observed during the morning until its maximum afternoon value. This study reported two maximum (early morning and afternoon time) and two minimum values (morning and evening time) of HGF_{85%}. As a consequence, the main reasons for this incremental behavior were, increase in the ratio of inorganic to OA and oxidation level, f44 ($m/z44/\text{OA}$) of the OA within the particle phase. In context to the effect of ambient RH, this study reported two distinct variations of mean HGF_{85%} as the function of ambient RH. The positive linear relationship at low RH (LRH, $RH \leq 50\%$) was clearly associated with low OA loading, relatively higher substantial temperature, and wind speed. We also observed increment in f44, and effective density indicating aging of aerosol. However, HGF_{85%} was found to inversely decline as a function of RH at higher RH (HRH, $RH > 50\%$) conditions, which clearly reflect the more significant

* Corresponding author at: Department of Civil Engineering, Indian Institute of Technology, Kanpur, India.

E-mail address: snt@iitk.ac.in (S.N. Tripathi).

contribution of primary OA and lower oxidation level of OA. Our results show the declining trend in size-resolved effective density at HRH conditions, confirming the above conclusions.

© 2019 Elsevier B.V. All rights reserved.

1. Introduction

Aerosol hygroscopic growth factor (HGF) depicts the response of aerosol's physical and chemical properties in atmospheric water uptake to varying relative humidity (RH) conditions. And, HGF at an ambient RH condition is essential because it can not only influence the secondary particle formation via aqueous-phase oxidation due to comparatively more availability of liquid water (Li et al., 2019; Mandariya et al., 2019; Xu et al., 2017) but also directly influence the observations of aerosol mass loading and compositions by influencing of impactor cut-off size (Chen et al., 2018), visibility (Charlson et al., 1967), and aerosol optical depth (AOD) (Attwood et al., 2014). However, its understanding is also essential in the global models to predict the size distribution better and scattering properties of aerosols under changing humidity conditions (Randall et al., 2007). Further, HGF is also linked to local visibility in high RH conditions. Since during hygroscopic growth at high RH conditions, the increased cross-sectional area of aerosols responsible for scattering light more effectively (Tang and Munkelwitz, 1994). The Hygroscopic Tandem Differential Mobility Analyzer (H-TDMA) system has mainly been used to determine the hygroscopic growth factors (HGF) of size-resolved aerosol particles.

Fast economic growth and industrialization in the Indo Gangetic Plain (IGP) in the past decades have led to bad air quality in this region during wintertime (Chowdhury et al., 2018; Nair et al., 2007; Wester et al., 2019). Hence, Kanpur, sitting on the center of IGP, is affected mainly by both local and regional air pollution problems in wintertime (Rai et al., 2016; Rajput et al., 2015, 2016). And, this high loadings of atmospheric aerosols in winter can lead to adverse acute and chronic health effects due to the penetration and deposition of submicron particles in the human respiratory system (Balakrishnan et al., 2019; Dandona et al., 2017; Singh and Gupta, 2016). Also, recent source apportionment studies at the current site revealed the biomass burning emission is a significant source to contribute OA loading in this region (Chakraborty et al., 2015; Chakraborty and Gupta, 2010; Mandariya et al., 2019). Besides, some studies, including the refractory part of aerosol (Rai et al., 2016; Rajput et al., 2016, 2015), indicate a lower fractional contribution of vehicular traffic emission mixed with vehicular resuspension dust. Besides, measurements of their hygroscopic properties at sub-saturated conditions, which are crucial for understanding their impact on regional visibility and fog formation, are not available. However, at IGP, hygroscopicity of ambient aerosols has been characterized via cloud condensation nuclei (CCN) counter, which is often coupled in the field with other instruments for bulk or size-resolve chemical composition measurements to explore the chemical link between hygroscopicity of particles and its chemical composition; instruments used in parallel or simultaneously include high-resolution time of flight aerosol mass spectrometer (HR-ToF-AMS, say AMS) (for bulk and size-resolve chemical composition) (Bhattu et al., 2016; Bhattu and Tripathi, 2014), and filter based high volume sampler (Patidar et al., 2012; Ram et al., 2014). However, few studies at locations in IGP explored only CCN based hygroscopicity and linked it with activation ratio (Roy et al., 2017). Furthermore, CCN, coupled with AMS based size-resolved hygroscopic studies, are in low time resolution and failed to capture local atmospheric chemistry in sub-saturated

ambient conditions. However, H-TDMA, parallelly coupled with AMS, has an advantage of high time resolution size-resolved HGF as well as it is a source of comprehensive chemical measurement that helps to explore the chemical link of aerosol with HGF. Although, H-TDMA is only able to provide hygroscopicity information of particles at desired specific sizes, which usually smaller than 350 nm in diameter (Wang and Chen, 2019). However, measurements of their hygroscopic properties at sub-saturated conditions, which are crucial for understanding their impact on regional visibility and fog formation, are currently not available from this part of the World. Although a study has been done using publicly available datasets in Delhi, India (Wang and Chen, 2019).

The hygroscopic growth factors of inorganic species have been thoroughly characterized and predicted, while HGF of the organic fraction remains highly uncertain because of the complex composition of organic aerosol and the scarcity of comprehensive laboratory and field data. HGF measurements have been carried out in various laboratory and field conditions around the globe. Out of these, several observational findings were related to the particle's hygroscopic properties and their link to chemical composition under different environmental background conditions (Chen et al., 2018; Hong et al., 2015, 2018; Tritscher et al., 2011). However, recent studies have principally centered on the HGF of OA, as ambient aerosols commonly contain numerous organic species, which exhibit various water uptake abilities. Various works considerably examined and reported the hygroscopic properties of the organic fraction in aerosols worldwide, including boreal forest (Hong et al., 2015), rural (Chang et al., 2010), and urban background areas (Mei et al., 2013; Wu et al., 2016). They observed that the oxidation level or oxygen to carbon ratio (O/C ratio) of organic aerosol (OA) is the significant factor that drives the water uptake ability of the OA fraction in aerosols. However, knowledge on the HGF and its dependence on the oxidation level of OA as well as on ambient RH in urban background areas under high aerosol mass loading conditions is very limited, for instance in India, where air pollution has become one of the top environmental concerns in recent decades (Cusworth et al., 2018) especially in fog dominated winter. Moreover, no one investigated the effect of ambient RH on size-resolved HGF (at particular RH) and density.

In this study, we measured the HGFs of accumulation mode particles (100 and 150 nm) and size-resolved chemical composition by a self-assembled hygroscopic tandem differential mobility analyzer (H-TDMA) and an high-resolution-time-of-flight mass spectrometer (HR-ToF-AMS), respectively, in Kanpur situated at the center of IGP. This study was carried out to investigate the effect of ambient RH and particles' chemical composition on the HGF of accumulation mode aerosol particles. Also, we focus on identifying the dependency of HGFs on the oxidation of OA and effective density of size-resolved aerosol.

2. Experimental methods

2.1. Aerosol measurements

Real-time atmospheric aerosol observations were made simultaneously with HR-ToF-AMS (say AMS) and H-TDMA in the winter season (27th November 2016 – 23rd January 2017) at the Indian

Institute of Technology (IIT) Kanpur in India (26.5°N , 80.3°E). The inlet for aerosol measurement was placed outside the window of the first floor in Centre for Environmental Science and Engineering (CESE) building at ~ 10 m above the ground level. Sampled aerosols were further dried (RH < 15%) in silica gel diffusion dryer and then divided into two-line, one line for AMS to measure the both bulk and size-resolved chemical composition of non-refractory submicron particles (NR-PM₁) and the second line for H-TDMA to measure the sub-saturated HGF of 100 and 150 nm particles at 85% RH. The AMS was operated in high-sensitivity V-mode at 600 °C vaporizer temperature for the time resolution of 2 min. The AMS was run alternatively in between two modes: in the mass spectrum (MS) mode the averaged chemical compositions were obtained by scanning *m/z* spectrum with time of flight (ToF) spectrometer without size information and in particle time of flight (PTOF) mode *m/z* based masses were obtained as function of aerodynamic vacuum diameter. The AMS was calibrated for ionization efficiency (IE) at 350 nm and particle sizing (40–600 nm) with NH₄NO₃ particles using a standard protocol. The IE calibration was carried out before, during, and after the winter campaign. More detailed explanations of the AMS measurement principles, mode of operations, and different calibrations can be found elsewhere (Canagaratna et al., 2007; Jayne et al., 2000; Jimenez et al., 2003). However, a significant drawback of AMS deployment is missing information on possibly hygroscopic fraction of refractory road dust and soil dust, which can cause the overestimation of fraction contribution of OA in NR-PM₁. Therefore, H-TDMA coupled parallelly with AMS could cause underestimation of hygroscopic growth of particles due to missing in the quantification of the salts of calcium, magnesium, and potassium, which might be both refractory and hygroscopic (Chen et al., 2018). However, Gupta and Mandariya (2013) observed crustal sources, contribute nearly 7% in PM₁ during winter at Kanpur. This contribution further possibly is low in accumulated size-specific particles, i.e., 100 and 150 nm, and might contribute non-significantly in size-resolved HGF_{85%}. As a result, these salts may contribute very low uncertainty in the measurement of accumulated size-specific HGF_{85%} reported in subsequent text.

The schematic diagram of the H-TDMA system is shown in Fig. 1. The detailed description of the H-TDMA setup can be found elsewhere (Mishra et al., 2019). We are describing the H-TDMA setup briefly here. The dried polydisperse aerosols were sent to first differential mobility analyzer (DMA1, TSI 3080). The DMA1 alternatively selects four different mobility diameters (D_0) 100, 150, 200, and 250 nm at an aerosol flow rate of 0.3 lpm of the non-zero width of the transfer function. Each size stepping was done after 12 min alternatively. Selected monodisperse particles were subsequently exposed to 85% RH, in the aerosol humidifier (single Nafion membrane). Aerosol particles were induced through the interior of the membrane, while saturated particles free air flow sent through the outside of the membrane in counterflow conditions. The resulting grown particles of mobility diameter, D (RH), were measured with a Scanning Mobility Particle Sizer (SMPS, TSI-3082) consisting of a second DMA2 (TSI-3080) to measure size and a Condensation Particle Counter (CPC, TSI-3776) to measure the particle number concentration respectively. The increase in particle size ($D(\text{RH})/D_0$) is defined as the hygroscopic growth factor (HGF) of particles. Measurements of DMA2 and CPC in the space of GF is defined as measurement distribution function (MDF). MDF covered all the GF range, which can be obtained by size ($D(\text{RH})$) scanning with DMA2 while keeping DMA1 at uniform size-selective mode (D_0). One full H-TDMA scan time was 6 min, out of 6 min, 5 min was DMA2 scan time, and rest 1 min was kept for purging to avoid artifacts between two scans. DMA2 sheath airflow is introduced through the DMA2 sheath flow humidifier (multiple Nafion membranes), circulating through the outside of the membranes to minimize pressure drops. Saturated airflow circulates through the interior of the membrane, flowing from top to the bottom. A saturated airflow (5–6 lpm) is generated with the heated water saturator. The temperature of circulating water between ambient conditions to 60 °C is controlled by a Proportional-Integral-Derivative (PID) device. Depending on the RH set-point on Ramp & Soak controller, the 3-way valve mixes the saturated airflow with dry compressed particle-free air. The accuracy and performance of the H-TDMA measured with pure ammonium sulfate aerosols (purity: 99.99%, Sigma-Aldrich), which

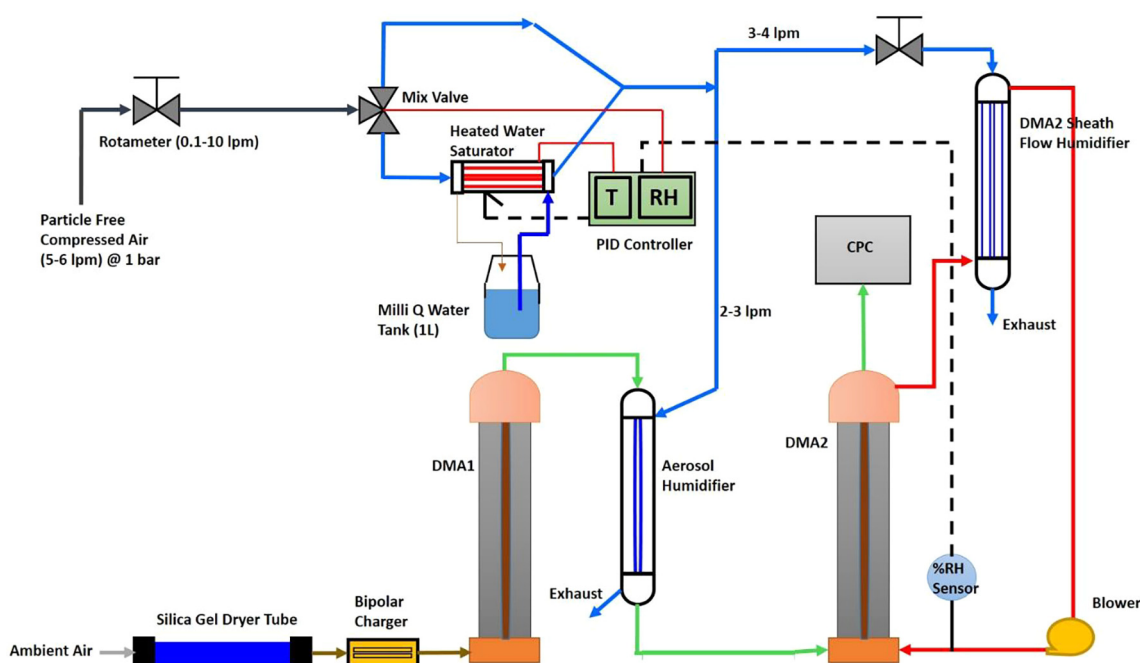


Fig. 1. The schematic diagram of the H-TDMA system.

has well-known GFs for 100 nm at 85% RH before the campaign. However, aerosol sample drying below 15% RH, was responsible for the loss of semi-volatile compounds. The evaporation of particulate NH_4NO_3 mostly occurred in between DMA1 and DMA2 sections cause negative artefacts because of its volatile nature. This evaporation loss of NH_4NO_3 can be minimized by keeping line temperature low, short residence time (Gysel et al., 2007) or/and RH around 30–40% (Wang and Chen, 2019; WMO/GAW, 2016). However, Wu et al. (2016) have observed that these negative artefacts due to NH_4NO_3 evaporation could be reduced by restricting data points with the volume fraction of NH_4NO_3 and OA below 20% and higher than 50%, respectively. Here, this study observed that the overall mean volume fraction of NH_4NO_3 and OA were 0.12 ± 0.05 (mean \pm 1 standard deviation), and 0.84 ± 0.07 , respectively for 100 nm particles whereas for 150 nm particles they were 0.15 ± 0.04 , 0.80 ± 0.06 , respectively. Furthermore, the volume fractions of NH_4NO_3 and OA in both size particles were observed well within the limit reported by Wu et al. (2016), possibly indicative of the fact that HGF_85% reported in subsequent text were less influenced with negative artefacts of NH_4NO_3 evaporation.

Throughout the whole campaign period, ambient RH and temperature measured by using a temperature and RH sensor (Vaisala, Inc. HUMICAP, HMT331 accuracy of $\pm 1\%$ for $\text{RH} < 90\%$ and $\pm 1.7\%$ for $90\% \leq \text{RH} < 100\%$ RH). Deng et al. (2008) observed nearly 5% of negative bias in RH measurement by instrument under extremely high RH conditions. Wind speed (WS), and wind direction (WD) measured with a time resolution of 30 min average (Sensors: iNGEN, accuracy: $\pm 0.5 \text{ ms}^{-1}$ (WS), $\pm 5^\circ$ (WD)). The windrose plot was drawn by openair in R package (<http://www.r-project.org>, <http://www.openair-project.org>). The 48 h back trajectory (BT) of air masses reaching Kanpur site at 500 m above the ground at every hour for the entire study period was estimated by an offline based Hybrid Single-Particle Lagrangian Integrated Trajectory (HYSPLIT4) model developed by NOAA/Air Resources Laboratory (ARL) (Draxler and Rolph, 2003). The input meteorological data for BT analysis were taken from the Global Data Assimilation System (GDAS 0.5) archive maintained by ARL (<http://ready.arl.noaa.gov/archives.php>). After that, by utilizing these estimated BT as input combined with the measured mass fraction of chemical species of D_{100} and D_{150} particles, Potential Source Contribution Function (PSCF) analysis was carried out with the help of a tool called Zefir (V 3.7) written in Igor Pro (WaveMetrics). Detail description regarding the Zefir tool can be found elsewhere (Petit et al., 2017).

2.2. Validation of H-TDMA

To validate the H-TDMA system, pure ammonium sulphate ($(\text{NH}_4)_2\text{SO}_4$) particles were produced by an atomizer (TOPAS atomizer) and a humidogram is established for 100 nm dry electrical mobility diameter particles to compare with theoretical calculations according to the reported method for H-TDMA calibration (Gysel et al., 2007; Sjogren et al., 2007; Topping et al., 2005; Villani et al., 2008). DMA1 was kept at a constant voltage to select a 100 nm dry mobility diameter. The measurements were made at 60, 70, 80, 85, and 90% RH to study the humidogram. The measured and calculated growth factors closely matched within the uncertainty range (± 0.04) and can be found elsewhere (Mishra et al., 2019).

2.3. Data analysis

2.3.1. H-TDMA data analysis

A detailed description of the H-TDMA data analysis procedure is described elsewhere (Gysel et al., 2009) accordingly, only a brief outline is given here. In this study, the sample flow rate and sheath to sample flow ratio were kept as 0.3 lpm and 10, respectively, in

H-TDMA. H-TDMA calibration was done at the start, during, and end of the measurement period by ammonium sulfate (purity: 99.99%, Sigma-Aldrich) particles. The raw data of H-TDMA is then processed according to the procedure and inversion routine described by Gysel et al. (2009). A piecewise linear TDMAinv algorithm developed by Gysel et al. (2009) was used to measure growth factor probability density functions (GF-PDFs) from the measurement distribution function (MDF). This approach uses a full TDMA transfer forward function to retrieve the GF-PDF from the MDF function with a χ^2 minimization algorithm. Here, the growth factor (GF) resolution chosen was $\Delta G = 0.15$ to minimize the normalized χ^2 value. GF distribution scans at lower than 80% or higher than 90% RH were ignored. All filtered GF-PDF ($80\% < \text{RH} < 90\%$) were further corrected to $\text{RH} = 85\%$ following Eqs. (3) and Eqs. (6) in Gysel et al. (2009). Further, the hygroscopicity factor (κ value, here say $\kappa_{\text{H-TDMA}}$) of size-resolved aerosol from H-TDMA HGF_85% was calculated by equation (1) defining κ (kappa)-Köhler theory (Enroth et al., 2018; Petters and Kreidenweis, 2007) while hygroscopicity parameter associated with OA determined by simple mixing rule (equation (2)) method (Ogawa et al., 2016; Petters and Kreidenweis, 2007).

$$\kappa_{\text{H-TDMA}} = \left(\text{HGF}_{85\%}^3 - 1 \right) \left[\frac{1}{S} \exp \left(\frac{4\sigma M_w}{RT\rho_w D_0 \text{HGF}_{85\%}} \right) - 1 \right] \quad (1)$$

where $\kappa_{\text{H-TDMA}}$ is the hygroscopicity factor (kappa, κ value), $\text{HGF}_{85\%}$ is the HGF of D_0 particle at 85% RH, S is the saturation ratio of water and assume, $S = \text{RH}$ (in fraction), σ is the surface tension of the aerosol liquid droplet-air interface at the droplet composition in N/m and can be assumed similar to pure water, R is the universal gas constant in $\text{J K}^{-1} \text{ mol}^{-1}$, M_w is the molecular mass of water, T is the ambient temperature in Kelvin (K), ρ_w is the density of water in kg m^{-3} , and D_0 is the dry mobility diameter of the particle in m.

$$\kappa_{\text{H-TDMA}} = \varepsilon_{\text{NH}_4\text{NO}_3} \kappa_{\text{NH}_4\text{NO}_3} + \varepsilon_{(\text{NH}_4)_2\text{SO}_4} \kappa_{(\text{NH}_4)_2\text{SO}_4} + \varepsilon_{\text{OA}} \kappa_{\text{OA}} \quad (2)$$

$$\text{ALW}_{\text{OA}} = V_{\text{OA}} \kappa_{\text{OA}} \frac{\text{RH}}{(1 - \text{RH})} \quad (3)$$

where $\varepsilon_{\text{NH}_4\text{NO}_3}$, $\varepsilon_{(\text{NH}_4)_2\text{SO}_4}$, and ε_{OA} are the volume fraction of NH_4NO_3 , $(\text{NH}_4)_2\text{SO}_4$, and OA, respectively, $\kappa_{\text{NH}_4\text{NO}_3}$, $\kappa_{(\text{NH}_4)_2\text{SO}_4}$, and κ_{OA} are the respective hygroscopicity parameters (κ value), and V_{OA} is the volume concentration of OA. The size-resolved aerosol liquid water content ($\text{ALW}_{\text{inorg}}$) as a function of inorganic species mass concentration, ambient temperature (T), and RH, calculated by ISORROPIA-II model (Fountoukis and Nenes, 2007) while ALW associated with OA (ALW_{OA}) was calculated by equation (3) (Petters and Kreidenweis, 2007). ALW of size-resolved aerosol particles calculated by arithmetic addition of ALW associated with inorganics and OA of aerosol particles.

2.3.2. AMS data processing and size-resolve chemical characterization

AMS unit mass resolution (UMR) and high-resolution (HR) data were analyzed using AMS data analysis toolkit SQUIRREL (v1.62 D) and PIKA (v1.22 D), respectively. The AMS measured the particle size from 40 nm to 700 nm vacuum aerodynamic diameter (DeCarlo et al., 2004) with 100% transmission efficiency. The high-resolution data in v-mode were obtained by HR fitting up to 150 m/z and were used for elemental ratio measurement of OA (Aiken et al., 2008, 2007). The details of the AMS data processing procedure can be found elsewhere (Canagaratna et al., 2007; DeCarlo et al., 2006). The different mass concentrations of inorganic salts derived from UMR mass concentration of inorganics species (Gysel et al., 2007). The volume fraction of species and effective density of particles varies with particle size. Therefore volume-fraction-weighted effective densities were calculated for

bulk aerosol and each size by assuming a dynamic shape factor of one. The organic density of bulk OA obtained based on HR O:C and H:C atomic ratio of OA (Kuwata et al., 2012). Size-resolved mass was derived by performing the integration over the size ranges of 133–175 and 198–250 nm in D_{va} corresponding to the geometric mean of electrical mobility diameter 100 and 150 nm respectively (Kawana et al., 2017; Yeung et al., 2014). AMS measured the size-resolved mass of particles in terms of vacuum aerodynamic diameter (D_{va}) while H-TDMA gives the HGFs based on electrical mobility diameter (D_m). Therefore each D_{va} size was converted into D_m size (Zelenyuk et al., 2006).

The degree of oxygenation of OA can be calculated from the ion fragments in the organic unit mass resolution (UMR) mass spectra. The $m/z44$ (mass to charge ratio = 44) signal in UMR is mostly recognized in the ion fragment CO_2^+ and has been used as a tracer for low volatile oxygenated organic aerosols (LV-OOA). Moreover, the $m/z43$ signal in UMR is associated with the less oxidized $\text{C}_2\text{H}_3\text{O}^+$ and hydrocarbon C_3H_7^+ fragments. However, due to a relatively higher contribution of $\text{C}_2\text{H}_3\text{O}^+$ into $m/z43$, it has been used as a tracer of semi-volatile oxygenated organic aerosol (SV-OOA). Also, $m/z60$ fragment ion in mass spectra has been recognized as a tracer of levoglucosan, which is a marker of biomass burning OA (BBOA). Hydrocarbon-like OA associated with vehicular emission can be identified by the fragment ion $m/z57$ in UMR, which shows the presence of an alkyl fragment (mainly C_4H_9^+) (Canagaratna et al., 2007; Ng et al., 2011a). Consequently, the size-resolved mass fractions of these four ion fragments in the organic UMR mass spectra (f43, f44, f57, and f60) were obtained from the ratio of the corresponding m/z signal to the total OA signal and were expressed as a marker of SV-OOA, LV-OOA, HOA, and BBOA, respectively.

3. Result and discussion

3.1. Aerosol hygroscopic growth factor (HGF_85%) and Size-Resolved chemical composition

Figs. 2 and 3 show the time series of hourly averaged meteorological parameter (in each top two panels (a) and (b)) (relative humidity (RH), temperature (T), wind speed (WS), and wind direction (WD)), HGF_85% (in each top third panel (c)) and aerosol chemical properties (in each lower two panels (d) and (e)) of 100 (D_{100}) and 150 nm (D_{150}) D_o particles respectively measured during the winter field campaign. Meteorological parameters give an overview of weather conditions at the study site. The ambient temperature varied from 3.9 to 27.9 °C (mean \pm 1 standard deviation: 14.7 ± 4.0). Relative humidity varied from 21.4 to 100% ($77.9 \pm 17.3\%$). This variation in RH affects the particle physical form in the atmosphere, i.e., solid, semi-solid, metastable, and liquid. Furthermore, wind speed remained low (mean \pm 1 standard deviation: 1.04 ± 0.8). Low wind speeds along with shallow planetary boundary layer height (PBL) responsible for a lower value of ventilation coefficient, prohibit vertical mixing, and that leads to the accumulation of aerosol as Mandariya et al. (2019) observed the lower value of ventilation coefficient at a similar location in winter season. HGF_85% of 100 ($\text{HGF}_{85\%100\text{nm}}$) and 150 nm ($\text{HGF}_{85\%150\text{nm}}$) aerosol particles varied from 1.14–1.49 (1.27 ± 0.06) and 1.18–1.63 (1.34 ± 0.07), respectively, as a result of changes into a mass fraction of its chemical constituents (Fig. 2(c, d) and 3(c, d)). Both sizes mean HGF_85% were found statistical different ($p < 0.05$). The overall organic aerosol (OA) loading of both size aerosol particles (D_{100}, D_{150}) varied from 0.2 to 27.6 and 0.6 to 30.5 $\mu\text{g}/\text{m}^3$ (mean \pm 1 standard deviation: $4.5 \pm 3.7, 7.8 \pm 5.0 \mu\text{g}/\text{m}^3$), respectively, followed by NH_4NO_3 ($0.8 \pm 0.6, 1.7 \pm 1.0 \mu\text{g}/\text{m}^3$), and $(\text{NH}_4)_2\text{SO}_4$ ($0.2 \pm 0.3, 0.6 \pm 0.5 \mu\text{g}/\text{m}^3$). Besides, the aerosol composition of both sizes of aerosol was significantly different from each other

($p < 0.05$). In addition, the mass fraction of OA varied from 0.46 to 1.00 (0.81 ± 0.08) and 0.50 to 0.95 (0.76 ± 0.07). Whereas, the mass fraction for NH_4NO_3 was (0.15 ± 0.06) and (0.18 ± 0.05), in D_{100} and D_{150} aerosol particles, respectively. Furthermore, the mass fraction of $(\text{NH}_4)_2\text{SO}_4$ was (0.04 ± 0.05) and (0.06 ± 0.04) in D_{100} and D_{150} aerosol particles, respectively. Both size aerosol mass loading was associated with low wind speed, low temperature, and high ambient RH (Figs. 2 and 3(a, b, and e)). The detailed description of the relative effects of chemical species will be discussed in a subsequent section. The mean effective density of D_{150} ($1.44 \pm 0.02 \text{ g/cm}^3$) aerosols was significantly ($p < 0.05$) higher than of D_{100} ($1.42 \pm 0.03 \text{ g/cm}^3$) particles. The higher density of D_{150} than D_{100} aerosol particles indicates the D_{150} aerosols are relatively more aged as compared to D_{100} aerosol particles (Rissler et al., 2014a). It was also observed that $\text{HGF}_{85\%150\text{nm}}$ were significantly ($p < 0.05$) larger than $\text{HGF}_{85\%100\text{nm}}$. This finding is consistent with previous studies (Sjogren et al., 2012; Yeung et al., 2014) as it is a size-dependent hygroscopic parameter. This size dependency behavior of HGF_85% was similar to higher inorganic to OA mass fraction ratio of larger size aerosols (D_{150}) as compared to lower size aerosol (D_{100}) (Fig. 2(d) and 3(d)). This can also be explained by the inorganics as a major water-soluble constituent in aerosol and thus measure the aerosol hygroscopic nature.

3.2. Diurnal variation

The diurnal variability in the HGF of 100 ($\text{HGF}_{85\%100\text{nm}}$) and 150 nm ($\text{HGF}_{85\%150\text{nm}}$) particles were found more complex. The diurnal dependency of the mean HGF value for all data of both sizes of the aerosol is shown separately in Figs. 4 and 5, respectively. Mean diurnal variability of $\text{HGF}_{85\%100\text{nm}}$ and $\text{HGF}_{85\%150\text{nm}}$ (Fig. 4(c) and 5(c)) showed relatively significant change during the daytime, and revealed a shape which corresponds to the typical daily-activity time pattern of inhabitants in cities, including particularly the biomass burning emission and road traffic in Kanpur (Chakraborty et al., 2018). It consists of two minima at approximately 9:00 (mean $\text{HGF}_{85\%100\text{nm}} = 1.247$, and $\text{HGF}_{85\%150\text{nm}} = 1.324$) and 19:00 (mean $\text{HGF}_{85\%100\text{nm}} = 1.231$ and $\text{HGF}_{85\%150\text{nm}} = 1.298$), which agree with the heaviest vehicle traffic (morning and evening rush hours). This diurnal pattern of the minimum values was also significantly well correlated with the maximum value of f55 (ratio of $m/z55$ to total OA concentration (with a correlation coefficient of $R_{100\text{nm}} = -0.19$ and $R_{150\text{nm}} = -0.86$ for 100 and 150 nm particle respectively) and f57 (ratio of $m/z57$ to total OA concentration (with a correlation coefficient of $R_{100\text{nm}} = -0.57$ and $R_{150\text{nm}} = -0.88$) as shown in Fig. 4(b) and 5(b), which is associated with hydrocarbon-like OA (HOA) (Ng et al., 2010). HOA in urban areas almost always associated with vehicular emissions and primary combustion sources (e.g., vehicular tailpipe exhaust, biomass burning emissions) (Duplissy et al., 2011), supported by peak value of f55, f57, and f60 (Ng et al., 2011) during corresponding time (Zhang et al., 2005). Primary combustion emitted nearly hydrophobic or less hygroscopic particles such as black carbon and OA emitted directly from local primary sources, which inversely affect the HGF_85% (Wang et al., 2018). Also, this minima of HGF_85% might be attributed to traffic dust and black carbon. In continuation some recent studies have observed a black carbon concentration peak at the same time during the morning and evening hours at the same location in wintertime (Kanawade et al., 2014; Shamjad et al., 2015) and reported that this peak in black carbon concentration attributed to the primary emissions, i.e., traffic, biomass burning emissions, and biofuel burning emissions in the local vicinity of the sampling site (Kanawade et al., 2014). One more recent study (Rai et al., 2016) at the same location in winter, observed vehicular emission mixed with crustal dust contribute nearly 11% in PM_1 . Also, the resuspension dust due to road traffic is combined

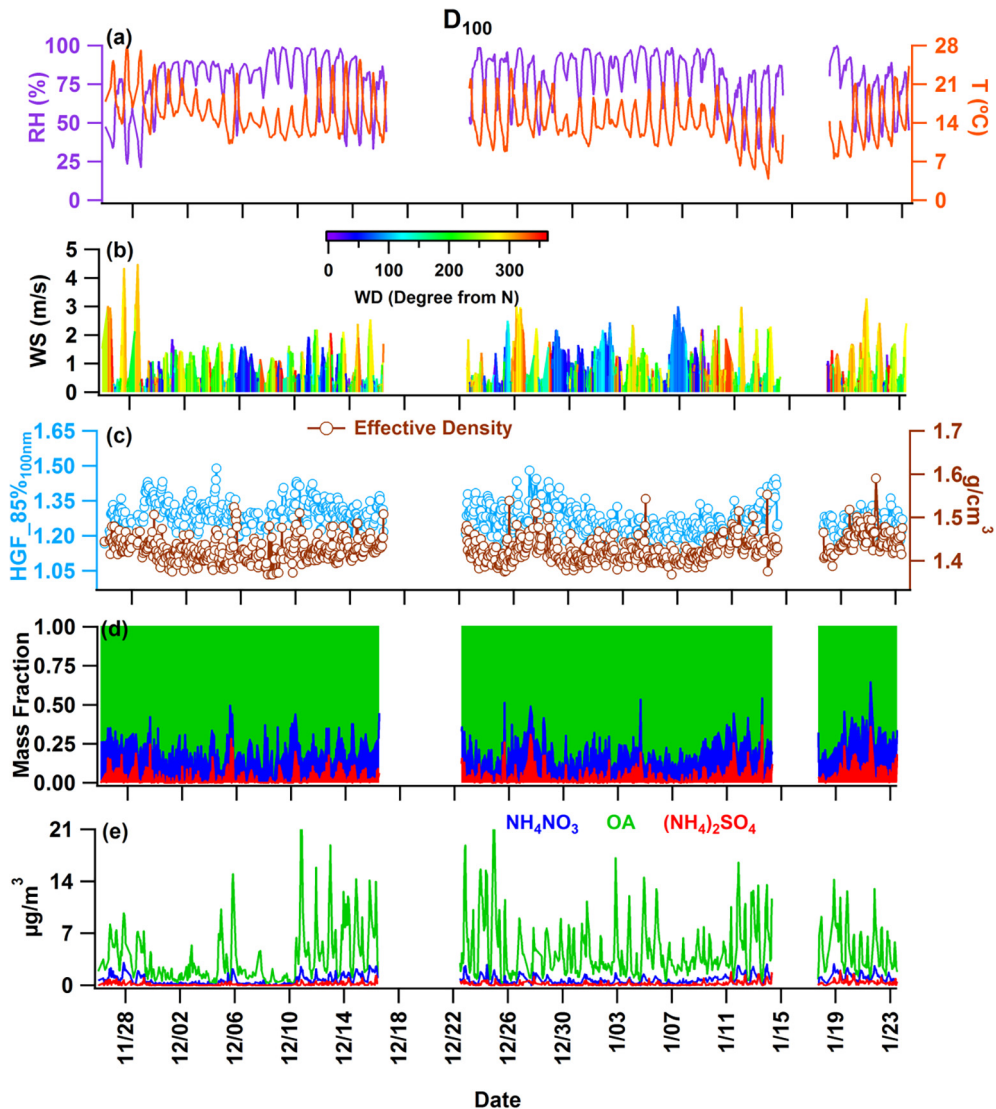


Fig. 2. The time series of (a) Relative humidity (RH), temperature (T), (b) wind speed (WS) and wind direction (WD), (c) effective density and hygroscopic growth factor (HGF_{85%}_{100nm}) of 100 nm size particles, (d) mass fraction of organic aerosol (OA), ammonium nitrate (NH_4NO_3), and ammonium sulfate ($(\text{NH}_4)_2\text{SO}_4$) of 100 nm size particles, and (e) mass concentration of organic aerosol (OA), ammonium nitrate (NH_4NO_3), and ammonium sulfate ($(\text{NH}_4)_2\text{SO}_4$) of 100 nm size particles.

with mineral dust, brake wear, tire wear, vehicular emissions, and construction dust (Aatmeeyata et al., 2009; Karanasiou et al., 2014). Further a laboratory study by Koehler et al. (2009) reported that size-selective particles of a different kind of mineral dust, i.e., Arizona test dust (100 and 200 nm diameter) and Saharan dust (200 nm diameter) exhibited very less HGFs (nearly hydrophobic) and possible due to restructuring of particle. This implies that the minimum value of HGF_{85%}_{100nm} and HGF_{85%}_{150nm} during diurnal variation was most probably due to vehicular emissions. Our κ_{HTDMA} values (Morning rush hour (0.098 ± 0.024 (100 nm)), 0.133 ± 0.025 (150 nm)); Evening rush hour (0.091 ± 0.022 (100 nm)), 0.121 ± 0.028 (150 nm))) also agree well with the κ value ($0.06 < \kappa < 0.12$) fresh and aged particles emitted from a diesel engine (Tritscher et al., 2011). The high mass fraction of OA (Fig. 4(c) and 5(c)) (correlation with HGF_{85%}_{100nm}, $R = -0.80$, $p < 0.05$ and HGF_{85%}_{150nm}, $R = -0.88$, $p < 0.05$) and f60 (ratio of m/z60 to total OA concentration, correlation with HGF_{85%}_{100nm}, $R = -0.52$, $p < 0.05$ and HGF_{85%}_{150nm}, $R = -0.91$, $p < 0.05$) also supports it. f60 is associated with biomass burning emissions (Ng et al., 2010), and a negative correlation of f60 and f73 signifies the effects of primary biomass burning OA (BBOA).

D_{100} and D_{150} size particles revealed their maximum HGF_{85%} in the early morning hours and minimum value during evening hours (Figs. 4 and 5, respectively). It can be explained by the noticeable slowdown in the strength of primary emission sources from midnight to early morning, as indicated by a substantial decrease in m/z55 and 57, f60, and f73. Also, considerable enhancement in the effective aerosol density due to continued aerosol processing during this time period supports it as well as signify the substantial aging of aerosol. These findings are different from those found in some other studies in urban air. Hong et al. (2015) observed the different diurnal variability than the present study for the same size of particles. Since they reported an evident diurnal variation of 100 and 145 nm size particles HGF, with lowest during the early morning hours (around 3:00 h), followed by a steady increase until afternoon, when it started to decrease further. These differences from the current study can be likely explained by the fact that the locations of study (Boreal forests emit enormous amounts of volatile organic compounds (VOCs)) and gas-phase chemistry of these VOCs, which produce condensing vapors and temperature-dependent gas-to-particle partitioning will be enhanced during the presence

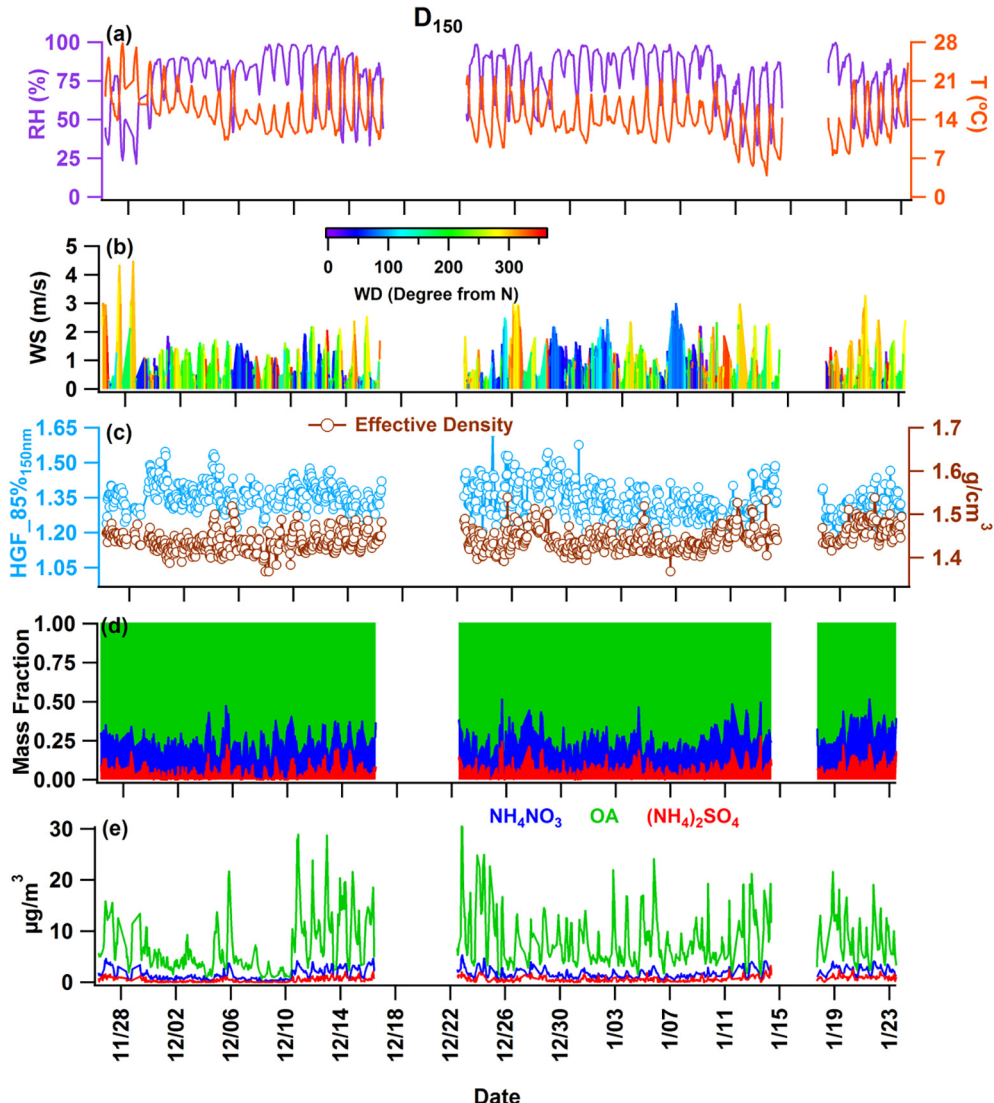


Fig. 3. The time series of (a) Relative humidity (RH), temperature (T), (b) wind speed (WS) and wind direction (WD), (c) effective density and hygroscopic growth factor ($HGF_{85\%150nm}$) of 150 nm size particles, (d) mass fraction of organic aerosol (OA), ammonium nitrate (NH_4NO_3), and ammonium sulfate ($(NH_4)_2SO_4$) of 150 nm size particles, and (e) mass concentration of organic aerosol (OA), ammonium nitrate (NH_4NO_3), and ammonium sulfate ($(NH_4)_2SO_4$) of 150 nm size particles.

of sunlight. Fan et al. (2019) also observed the minimum value of HGF_{150nm} in the nearly similar evening time (18:00 h) and attributed this values for a high fraction of hydrophobic particles reflects abundant primary OA (traffic emissions and cooking sources) during winter in urban Beijing although these measurements were carried out at 90% RH. Also, they found higher HGF during nighttime and early morning similar to the current study, due to the dominancy of more hygroscopic mode particles and attributed it with aqueous-phase oxidation or condensation process on pre-existing particles under lower temperature and higher RH. Also, (Chen et al., 2018a) reported a nearly similar diurnal pattern of $HGF_{85\%}$ for 100 nm wildfire haze particles. Furthermore, they found similar relationships of $HGF_{85\%}$ with inorganic to organic ratio, f44, f44/f43, OA, and BBOA. Furthermore, $HGF_{85\%}$ reconstructs its maximum value (1.295 (100 nm) and 1.403 (150 nm)) in the afternoon (15:00) following lower values in morning rush hours. This daytime enhancement in HGFs is clearly associated with photooxidation aging of aerosol. It can be supported by good correlation of diurnal variation of mean HGFs with f43 and f44, which are associated with semi-volatile oxygenated organic aerosol (SV-OOA) and low volatile oxygenated

organic aerosol (LV-OOA) respectively (Ng et al., 2011b). The f44 to f43 ratio increases during oxidation of OA (Ng et al., 2010). Although the comparatively higher solar radiation in afternoon hours favors more intense photooxidation processes and favor the partitioning of relatively more oxidized organics on the particulate surface under lower OA loadings than higher OA loadings. The diurnal variation of $HGF_{85\%}$ for both sizes exhibited good correlation with the diurnal ratio of f44 to f43, as shown in Fig. 4(b, c) and 5(b, c), supported the above findings. Also, the f44 started to increase after midnight and it peaked during the early morning and hence contributed in the enhancement of $HGF_{85\%}$ (Massoli et al., 2010; Duplissy et al., 2011) since the hygroscopicity of OA has been observed to be higher for larger f44 in laboratories study (Tritscher et al., 2011) and field study (Yeung et al., 2014).

The diurnal variation in ambient RH and ALWC also alter the chemical as well as oxidative properties of OA (Sun et al., 2013; Mandariya et al., 2019; Xu et al., 2017), causing changes in hygroscopicity of OA (Kawana et al., 2016), probably reflect to change in $HGF_{85\%}$. The relative effect of RH on $HGF_{85\%}$ will discuss in subsequent text. Further, effective density of both size of aerosol also

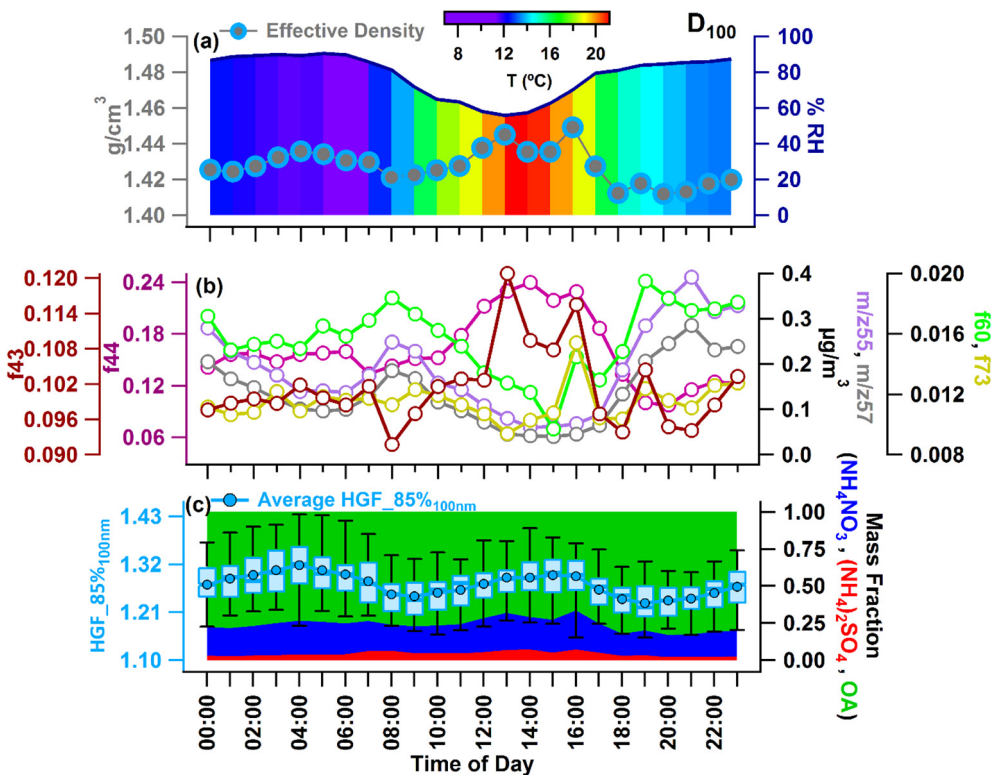


Fig. 4. Diurnal variation of (a) Relative humidity (RH), temperature (T), effective density of 100 nm size particles, (b) f43 (m/z 43/OA), f44 (m/z 44/OA), f55 (m/z 55/OA), f57 (m/z 57/OA), f60 (m/z 60/OA), and f73 (m/z 73/OA) of 100 nm size particles, and (c) hygroscopic growth factor ($HGF_{85\%100nm}$), mass fraction of organic aerosol (OA), ammonium nitrate ($(NH_4)_2NO_3$), and ammonium sulfate ($(NH_4)_2SO_4$) of 100 nm size particles.

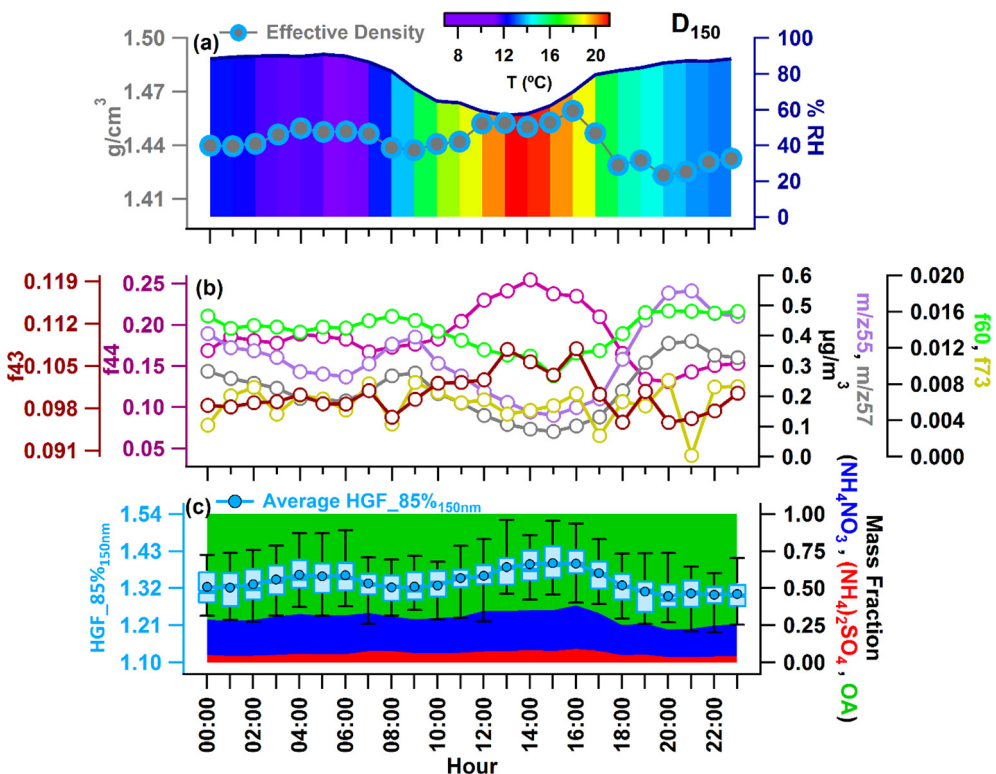


Fig. 5. Diurnal variation of (a) Relative humidity (RH), temperature (T), effective density of 150 nm size particles, (b) f43 (m/z 43/OA), f44 (m/z 44/OA), f55 (m/z 55/OA), f57 (m/z 57/OA), f60 (m/z 60/OA), and f73 (m/z 73/OA) of 150 nm size particles, and (c) hygroscopic growth factor ($HGF_{85\%150nm}$), mass fraction of organic aerosol (OA), ammonium nitrate ($(NH_4)_2NO_3$), and ammonium sulfate ($(NH_4)_2SO_4$) of 150 nm size particles.

revealed almost similar diurnal pattern as followed by HGF_85%, f43, and f44 (Fig. 4(a) and 5(a)) as during the aerosol aging process effective density of aerosol enhanced, moreover, primary particles exhibit lower density as compared to oxidized aerosol (Rissler et al., 2014b). The diurnal pattern of HGF_85% is also the reflection of changes in particle chemical composition. Also, analysis of variance (ANOVA) indicates statistically significant ($p < 0.05$) variation by time of day for HGFs and mass fraction of OA, NH_4NO_3 , and $(\text{NH}_4)_2\text{SO}_4$. The incremental behavior of HGF_85% during early morning and afternoon time also clearly associated with enhancement and decrement in the mass fraction of inorganic salts and OA, respectively, in particles (Kawana et al., 2016). Furthermore, this diurnal behavior also supported by variation of inorganic to organic (Hong et al., 2014). Also, 150 nm aerosol particles had a larger magnitude of hourly mean HGF_85% variability than the 100 nm particles.

3.3. Influence of ambient RH on HGF_85% and chemical composition

Fig. 6 illustrates the overall daytime mean variation of mass fraction of NR- PM_{1} species, OA evaluation markers (f43, f44, f57, and f60), and $\text{HGF}_{85\%100\text{nm}}$ and $\text{HGF}_{85\%150\text{nm}}$ separately, as a function of RH throughout the observed period. Both $\text{HGF}_{85\%100\text{nm}}$ and $\text{HGF}_{85\%150\text{nm}}$ observed two distinct trends at low RH levels (LRH) and high RH levels (HRH), as shown in Fig. 6(c and d). The overall $\text{HGF}_{85\%}$ appear positively and inversely linearly dependent as a function of RH at LRH ($\text{RH} \leq 50\%$), and HRH ($\text{RH} > 50\%$), respectively, reflects the substantial changes in the chemical properties of both size particles. However, mean $\text{HGF}_{85\%150\text{nm}}$ observed significantly ($p < 0.05$) higher than $\text{HGF}_{85\%100\text{nm}}$. Furthermore, in contrast, to examining this distinct $\text{HGF}_{85\%}$ variation with LRH and HRH, we plotted the chemical composition of aerosol particles, aerosol density, and OA evaluation markers (f43, f44, f57, and f60) as shown in Fig. 6. We found a statistically significant ($p < 0.05$) variation of all chemical species with RH. The two distinct variations in OA were observed at LRH and HRH. In the LRH domain, when ambient RH increases, OA fractional contribution reduce by 7% and 9% in D_{100} and D_{150} particles, respectively. Besides in HRH estate, it gets

enhanced nearly by 24% and 18% in 100 and 150 nm aerosol particles, respectively. This substantial increment indicates a change in the relative contribution of primary and secondary OA in particles. In continuation, to identify the type of OA component (primary or secondary) that contributed more to the HRH domain, we also evaluated f57, f60, f43, and f44 as a function of RH. We observed dominancy of secondary OA reduction in aerosol as indicated by the reduction of f43 (SV-OOA) and f44 (LV-OOA) by 20% and 31%, respectively, in D_{100} particles. Similarly, D_{150} particles also witnessed a reduction of 11% and 18% in f43 and f44, respectively. However, primary OAs, i.e., HOA and BBOA, contribution to OA, got raised in both size particles, supported by enhancement in f57 (HOA) and f60 (BBOA) by 20% and 43%, respectively in D_{100} particles and by 22% and 37%, respectively in D_{150} particles. Therefore, above results suggest that the relative enhancement in the loading of primary OA components as compared to fall in SOA contribution, most probably was responsible for the decline of $\text{HGF}_{85\%}$ of both size particles at HRH. Apart from, HOA contribution raised as indicated by an increment (69%) of f57 while BBOA shares decreased as f60 reduces by 23% in D_{100} particles at LRH. These two primary OA components most probably counteract each other's effects on $\text{HGF}_{85\%}$. In continuation, share of both SOA components SV-OOA and LV-OOA, overall increased in OA as indicated by an increment of 7% and 24% in f43 and f44, respectively. A similar trend also observed in D_{150} particles at LRH domain. The variation of an inorganic to organic ratio can also explain these different trends. The net increment by 31% (D_{100}), 39% (D_{150}), and decrement by nearly 63% (D_{100}) and 46% (D_{150}) in this ratio, also responsible for this type of trend (Hong et al., 2014). The inverse relationship of f60 to f43 and f44 also support these findings as these relationships indicate the negative impact of relatively fresh BBOA to HGF as fresh BBOA is less hygroscopic as compared to which more aged. These results are consistent with other worldwide studies (Duplissy et al., 2011; Hong et al., 2018). Furthermore, to observe the potential source for mass loading of varies chemical species, we performed PSCF by combining BTs with the mass fraction (mf) of different chemical species. Fig. 7 specifies the probability of potential sources related to the mass fraction of D_{100} particles

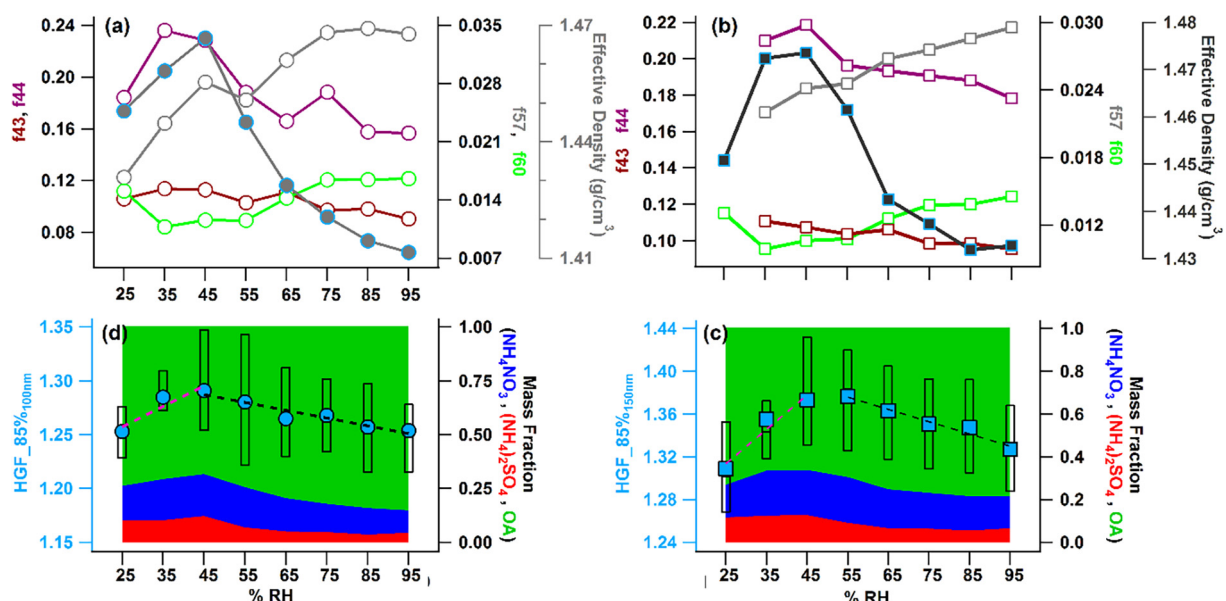


Fig. 6. Variation of daytime mean value various parameters (a), (b) effective density, f43 ($m/z 43/\text{OA}$), f44 ($m/z 44/\text{OA}$), f57 ($m/z 57/\text{OA}$), and f60 ($m/z 60/\text{OA}$), and (c), (d) hygroscopic growth factor ($\text{HGF}_{85\%}$), mass fraction of organic aerosol (OA), ammonium nitrate (NH_4NO_3), and ammonium sulfate ($(\text{NH}_4)_2\text{SO}_4$) as a function of ambient relative humidity (RH). The circle represents an RH bin averaged data point for 100 nm particles, whereas square indicates the RH bin averaged data points of 150 nm particles. The dotted line represents the regression line of $\text{HGF}_{85\%}$ Vs. %RH.

constituents (OA, NH_4NO_3 , and $(\text{NH}_4)_2\text{SO}_4$) and marker of OA factors (SV-OOA, LV-OOA, BBOA, and HOA) in terms of a color bar. Similar plots were observed for D_{150} particles also (not shown here). The areas with high probability values were explained as the potential area source of D_{100} particles constituents and OA factors. As shown in Fig. 7(b and h), NH_4NO_3 was transported to the site from distant locations source. Whereas, $(\text{NH}_4)_2\text{SO}_4$ aerosol was contributed from local sources. However, OA loading was dominated by nearby local sources, as illustrated in Fig. 7(a). In addition, LV-OOA, HOA, and BBOA at the site were governed largely by local sources (Fig. 7(h, d, and f, respectively). However, SV-OOA (Fig. 7(c)) was also influenced by distant sources in addition to local sources. It means that local emission sources

dominated the current site during wintertime. Also, as shown in Fig. 7(a, c, h, and e), the high OA loading source contributed to low oxygenated OA. Besides, the wind rose diagram, as shown in Fig. 7(e), indicates little influence of the distant regional sources.

Further to support the above conclusions, we plotted RH bin mean f44, f57, f60, the mass fraction of NR- PM_1 species, and aerosol density against the mean of RH bins HGF_85% as shown in Fig. 8. We found f43, f44, inorganics mass fraction, and aerosol density positively correlated with HGF_85% in the function of the RH bin. This is also supported above results and consistent with other studies (Massoli et al., 2010). Similarly, f57 and f60 also show a negative effect on HGF_85% (Fig. 8(c and f)). A possible

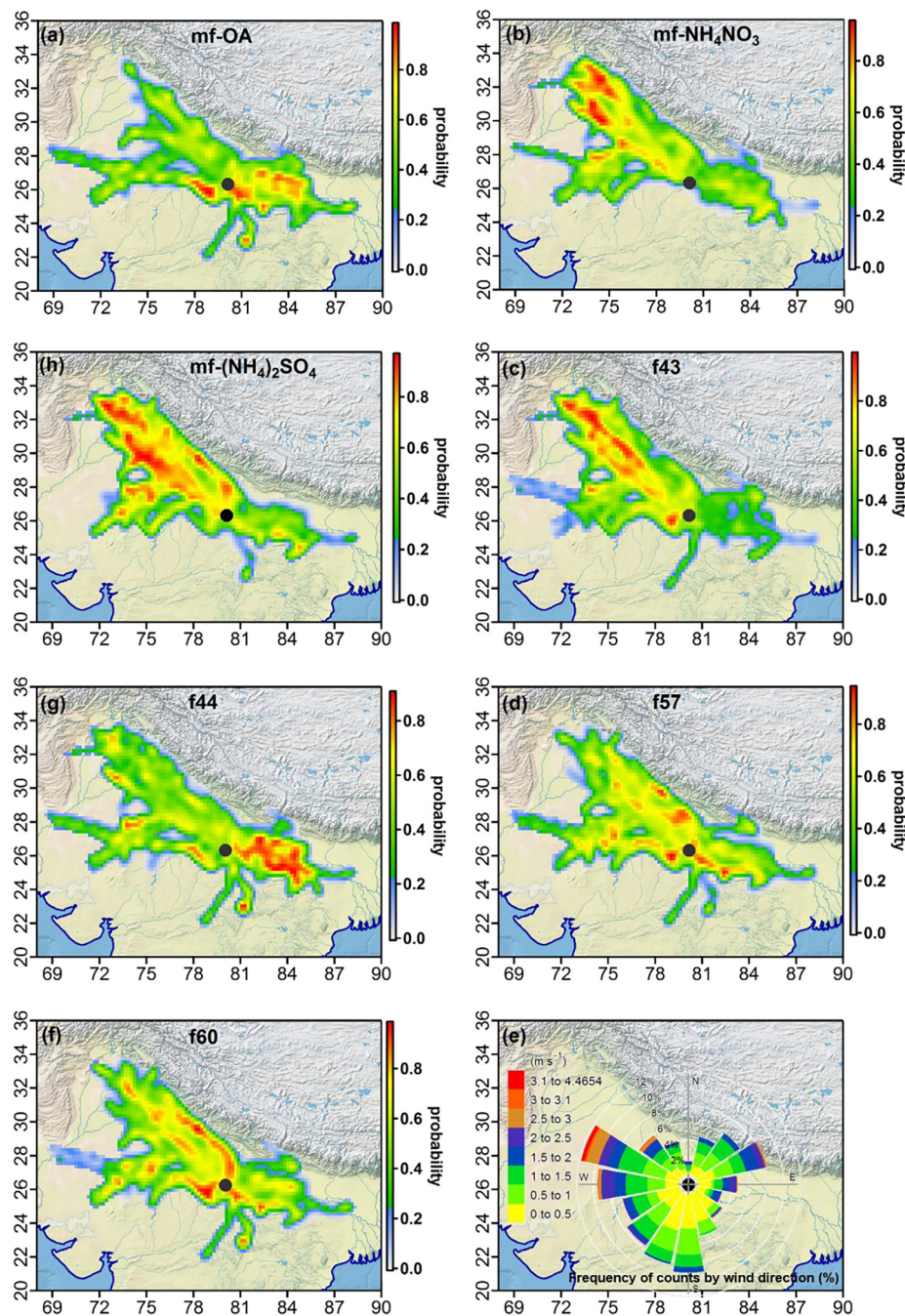


Fig. 7. Association of the relative mass contribution of various chemical species (a) organic aerosol (OA), (b) NH_4NO_3 , (c) f43 (m/z 43/OA), (d) f57 (m/z 57/OA), (f) f60 (m/z 60/OA), (g) f44 (m/z 44/OA), (h) $(\text{NH}_4)_2\text{SO}_4$, in 100 nm particles with air mass trajectories (BT), and (e) windrose diagram.

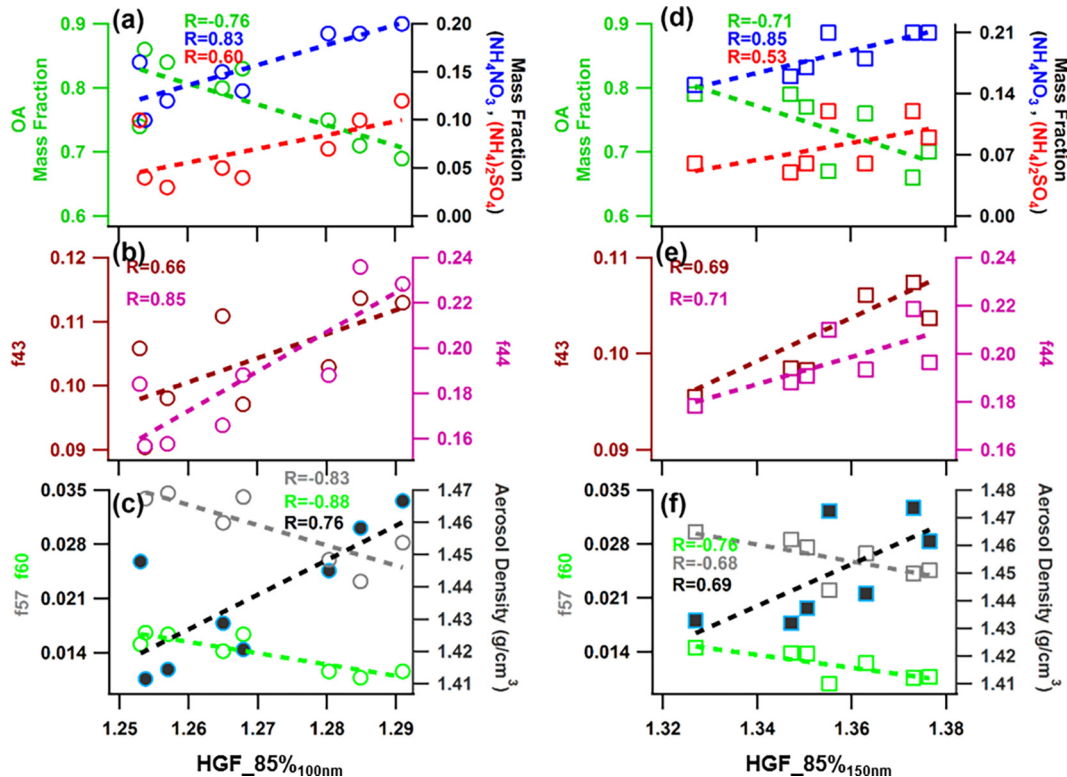


Fig. 8. Variation of daytime RH bin mean value of various parameter's (a), (d) mass fraction of OA, NH_4NO_3 , and $(\text{NH}_4)_2\text{SO}_4$, (b), (e) f43 (m/z 43/OA) and f44 (m/z 44/OA), and (c), (f) f57 (m/z 57/OA), f60 (m/z 60/OA), and aerosol density in the function of hygroscopic growth factors (HGF_85%). The circle represents a data point for 100 nm particles, whereas square indicates the data points of 150 nm particles. The color-coded dashed lines represent the regression line of the corresponding parameter with HGF_85%.

applicant for this effect could be carbonaceous material emitted from local automobile exhaust during rush hours, and nighttime biomass burning with soot and water-insoluble organics as the major components (Hong et al., 2018; Kawana et al., 2016). Furthermore, inorganic species mass fraction also showed a positive correlation with HGF_85%, consistent with the previous study at a similar location (Bhattu and Tripathi, 2015). And, inorganic to an organic ratio of particles is also a better way to explain these different trends of HGF_85% for LRH and HRH domain. At LRH, there was an overall increment in this ratio by 31% and 39% in D_{100} and D_{150} particles, respectively. Whereas, overall decrement of nearly 63% and 46% was observed in corresponding particle size (Hong et al., 2014). Inorganic salts are considered more hygroscopic than OA in nature; therefore, inorganic to an organic ratio indicates the hygroscopic nature of aerosol (Hong et al., 2014).

Fig. 6. Variation of daytime mean value various parameters (a), (b) effective density, f43 (m/z 43/OA), f44 (m/z 44/OA), f57 (m/z 57/OA), and f60 (m/z 60/OA), and (c), (d) hygroscopic growth factor (HGF_85%), mass fraction of organic aerosol (OA), ammonium nitrate (NH_4NO_3), and ammonium sulfate ($(\text{NH}_4)_2\text{SO}_4$) as a function of ambient relative humidity (RH). The circle represents an RH bin averaged data point for 100 nm particles, whereas square indicates the RH bin averaged data points of 150 nm particles. The dotted line represents the regression line of HGF_85% Vs. %RH.

Further, to evaluate the effect of aqueous-phase processing on the aerosol's HGF, we looked relation of volume fraction of aerosol liquid water content (ALW_{VF}) in NR- PM_1 with HGF and aerosol properties. The ALW_{VF} varies substantially from around 10 to 74%. We observed mean RH bin OA mass fraction enhancement in both sizes of the aerosol is also positively well correlated to ALW_{VF} , as

shown in Table S1. In subsequent, f60 (BBOA) and f57 (HOA) dominancy increases as a function ALW_{VF} , also supported by the good positive correlation of f60 and f57, respectively, with ALW_{VF} . This can be explained by enhancement in the condensation process during relatively higher RH and lower T environment at higher RH bins, which could be responsible for a better driving force to grow the particles via condensation (Seinfeld and Pandis, 2006). ALW is an abundant aerosol constituent and remains present in the condensed phase at the aerosol surface as a function of RH, temperature, and aerosol chemical composition (Zhou et al., 2011). Mandariya et al. (2019) reported OA loading as well as BBOA mass fraction in OA, enhanced during high RH and low T environment in wintertime, and alter the oxygen to carbon ratio either positively or negatively at the current site. This positive and negative impact on oxygen to carbon ration depends on the proportional contribution enhancement in primary OA and secondary OA (Mandariya et al., 2019) as high ALWC also favored the aqueous-phase formation pathway of SOA (Xu et al., 2017). Besides, f44 (a marker of LV-OOA) and f43 (SV-OOA) were showed an inverse correlation with ALW_{VF} (Table S1). This correlation probably indicated the relatively more considerable contribution of primary OA over the formation of SOA in the presence of larger ALW_{VF} . However, the f44 indicates the aging of OA. So, as a reflection of it, probably HGF showed increasing trend at LRH due to decline in OA loading, while negative trend at HRH, which has shown the negative impact on the oxygen to carbon ration of OA (Chakraborty et al., 2016). Worldwide many studies showed positive linear relationship of hygroscopicity factor (κ) with oxygen to carbon ratio of OA (Hong et al., 2018; Kawana et al., 2016; Cerully et al., 2015; Sjogren et al., 2012; Duplissy et al., 2011; Massoli et al., 2010). Also, Bhattu and Tripathi (2015) reported a positive linear relationship between κ and oxygen to carbon ration of OA at the current location.

4. Conclusions

In this study, hygroscopic growth factors (HGF_85%) at 85% RH were quantified for ambient aerosol particles with dry mobility diameters of 100 and 150 nm in situ by using an H-TDMA system in Kanpur, situated at the center of IGP during fog dominated winter time. The HGF_85% measurements were supported by an HR-ToF-AMS to obtain information on the size-resolved chemical composition of the aerosols and meteorological sensors, which were operated in parallel. We reported temporal variation in H-TDMA based HGF_85% first time in India. Our study is emphasizing the role of ambient RH on the HGF_85% and chemical composition of 100 and 150 nm aerosol particles. IGP faces several fog episodes every year during winter, which adversely impacts on the human health, climate, air quality, and economy of the region.

The observed HGF_85% at 85% RH ranged from 1.14 to 1.49 (HGF_85%_{100nm}, mean: 1.27 ± 0.06) and 1.18 to 1.63 (HGF_85%_{150nm}, mean: 1.34 ± 0.07) for 100 and 150 nm aerosol particles, respectively. This mean value of HGF_85%_{100nm} was significantly lower than that of the mean value of HGF_85%_{150nm}. The higher value of HGF_85%_{150nm} than HGF_85%_{100nm} indicates that 150 nm particles retain more liquid water than 100 nm particles per unit of dry volume, which probably is associated with the particle's chemical composition (Raoult effect). Besides 100 nm (mean inorganic to OA ratio: 0.25 ± 0.14), aerosol particles were more enriched with organics as compared to 150 nm (mean inorganic to OA ratio: 0.33 ± 0.14) particles.

The HGF_85% of both size particles revealed an evident dynamic variation, consists of two minima, followed the typical diurnal pattern of heavy vehicle traffic (morning and evening rush hours), local biomass burning emissions, and the mixing of locally emitted and long-range transported aerosols. Moreover, an enhancement to the HGF_85% from morning minimum value to the maximum afternoon value reflects the consequence of partially oxidized organic compounds and relatively significant-high inorganic content.

In contrast to the impact of ambient relative humidity on the HGFs, we observed two distinct relationships between mean HGF_85% and RH, first positive linear at LRH ($RH \leq 50\%$) and second inverse linear at HRH ($RH > 50\%$). LRH relationship was clearly associated with a larger inorganic to organic ratio, and a high contribution of SV-OOA (f43) and LV-OOA (f44). However, HRH inverse relationship revealed to lower inorganic to organic ratio and higher contribution of HOA (f57) and BBOA (f60). Also, HRH periods were associated with high aerosol loading and high ALW_{VF}. We also reported that the mean values of HGF as a function of RH of both size particles were positively correlated to inorganic mass fraction, oxygenated OA marker (f43 and f44), and aerosol particle density while inversely correlated to OA mas fraction, and primary OA marker (f57 and f60).

Declaration of Competing Interest

The authors declare that they have no known competing financial interests or personal relationships that could have appeared to influence the work reported in this paper.

Acknowledgment

The authors appreciatively acknowledge the financial support from the Board of Research in Nuclear Science (BRNS), Department of Atomic Energy (DAE), Government of India to provide the H-TDMA system for this research under project no. 36 (2,4)/15/01/2015-BRNS. We also acknowledge the support of IIT Kanpur for providing us with HR-ToF-AMS for PG research and

teaching. The authors also thankful to Dr. Martin Gysel, Aerosol Physics Group, Paul Scherrer Institute, Switzerland, for providing TDMAinv toolkit for HTDMA data correction. We also sincerely thank the editor for handling the manuscript and the reviewers for reviewing the manuscript.

Appendix A. Supplementary data

Supplementary data to this article can be found online at <https://doi.org/10.1016/j.scitotenv.2019.135363>.

References

- Aatmeeayata, Kaul, D.S., Sharma, M., 2009. Traffic generated non-exhaust particulate emissions from concrete pavement: a mass and particle size study for two-wheeler and small cars. *Atmos. Environ.* 43, 5691–5697. <https://doi.org/10.1016/j.atmosenv.2009.07.032>.
- Aiken, A.C., DeCarlo, P.F., Jimenez, J.L., 2007. Elemental analysis of organic species with electron ionization high-resolution mass spectrometry. *Anal. Chem.* 79, 8350–8358. <https://doi.org/10.1021/ac071150w>.
- Aiken, A.C., Decarlo, P.F., Kroll, J.H., Worsnop, D.R., Huffman, J.A., Docherty, K.S., Ulbrich, I.M., Mohr, C., Kimmel, J.R., Sueper, D., Sun, Y., Zhang, Q., Trimborn, A., Northway, M., Ziannia, P.J., Canagaratna, M.R., Onasch, T.B., Alfarra, M.R., Prevot, A.S.H., Dommen, J., Duplissy, J., Metzger, A., Baltensperger, U., Jimenez, J.L., 2008. O/C and OM/OC Ratios of O/C and OM/OC ratios of primary, secondary, and ambient organic aerosols with high resolution time-of-flight aerosol mass spectrometry. *Environ. Sci. Technol.* 42, 4478–4485.
- Attwood, A.R., Washenfelder, R.A., Brock, C.A., Hu, W., Baumann, K., Campuzano-Jost, P., Day, D.A., Edgerton, E.S., Murphy, D.M., Palm, B.B., McComiskey, A., Wagner, N.L., de Sá, S.S., Ortega, A., Martin, S.T., Jimenez, J.L., Brown, S.S., 2014. Trends in sulfate and organic aerosol mass in the Southeast U.S.: Impact on aerosol optical depth and radiative forcing. *Geophysical Research Letters* 41 (21), 7701–7709. <https://doi.org/10.1002/2014GL061669>. In this issue.
- Balakrishnan, K., Dey, S., Gupta, T., Dhaliwal, R.S., Brauer, M., Cohen, A.J., Stanaway, J., Beig, G., Joshi, T.K., Aggarwal, A.N., Sabde, Y., Sadhu, H., Frostad, J., Caseyy, K., Godwin, W., Shukla, D.K., Kumar, G.A., Varghese, C.M., Muraleedharan, P., Agrawal, A., Anjana, R.M., Bhansali, A., Bhardwaj, D., Burkart, K., Cercy, K., Chakma, J.K., Chowdhury, S., Christopher, D.J., Dutta, E., Furtado, M., Ghosh, S., Ghoshal, A.G., Glenn, S.D., Guleria, R., Gupta, R., Jeemon, P., Kant, R., Kant, S., Kaur, T., Koul, P.A., Krish, V., Krishna, B., Larson, S.L., Madhipatla, K., Mahesh, P., A., Mohan, V., Mukhopadhyay, S., Mutreja, P., Naik, N., Nair, S., Nguyen, G., Odell, C.M., Pandian, J.D., Prabhakaran, D., Prabhakaran, P., Roy, A., Salvi, S., Sambandam, S., Saraf, D., Sharma, M., Shrivastava, A., Singh, V., Tandon, N., Thomas, N.J., Torre, A., Xavier, D., Yadav, G., Singh, S., Shekhar, C., Vos, T., Dandona, R., Reddy, K.S., Lim, S.S., Murray, C.J.L., Venkatesh, S., Dandona, L., 2019. The impact of air pollution on deaths, disease burden, and life expectancy across the states of India: the Global Burden of Disease Study 2017. *Lancet Planet. Heal.* 3, e26–e39. [https://doi.org/10.1016/S2542-5196\(18\)30261-4](https://doi.org/10.1016/S2542-5196(18)30261-4).
- Bhattu, D., Tripathi, S.N., 2015. CCN closure study: effects of aerosol chemical composition and mixing state. *J. Geophys. Res. Atmos.* 120, 766–783. <https://doi.org/10.1002/2014JD021978>.
- Bhattu, D., Tripathi, S.N., 2014. Inter-seasonal variability in size-resolved CCN properties at Kanpur, India. *Atmos. Environ.* 85, 161–168. <https://doi.org/10.1016/j.atmosenv.2013.12.016>.
- Bhattu, D., Tripathi, S.N., Chakraborty, A., 2016. Deriving aerosol hygroscopic mixing state from size-resolved CCN activity and HR-ToF-AMS measurements. *Atmos. Environ.* 142, 57–70. <https://doi.org/10.1016/j.atmosenv.2016.07.032>.
- Canagaratna, M.R., Jayne, J.T., Jimenez, J.L., Allan, J.D., Alfarra, M.R., Zhang, Q., Onasch, T.B., Drewnick, F., Coe, H., Middlebrook, A., Delia, A., Williams, L.R., Trimborn, A.M., Northway, M.J., DeCarlo, P.F., Kolb, C.E., Davidovits, P., Worsnop, D.R., 2007. Chemical and microphysical characterization of ambient aerosols with the aerodyne aerosol mass spectrometer. *Mass Spectrom. Rev.* 26, 185–222. <https://doi.org/10.1002/mas.20115>.
- Cerully, K.M., Bougiatioti, A., Hite, J.R., Guo, H., Xu, L., Ng, N.L., Weber, R., Nenes, A., 2015. On the link between hygroscopicity, volatility, and oxidation state of ambient and water-soluble aerosols in the southeastern United States. *Atmos. Chem. Phys.* 15, 8679–8694. <https://doi.org/10.5194/acp-15-8679-2015>.
- Chakraborty, A., Bhattu, D., Gupta, T., Tripathi, S.N., Canagaratna, M.R., 2015. Real-time measurements of ambient aerosols in a polluted Indian city: Sources, characteristics, and processing of organic aerosols during foggy and nonfoggy periods. *J. Geophys. Res. Atmos.* 120, 9006–9019. <https://doi.org/10.1002/2015JD023419.Received>.
- Chakraborty, A., Gupta, T., 2010. Chemical characterization and source apportionment of submicron ($PM_{2.5}$) aerosol in Kanpur Region, India. *Aerosol Air Qual. Res.* 10, 433–445. <https://doi.org/10.4209/aaqr.2009.11.0071>.
- Chakraborty, A., Gupta, T., Tripathi, S.N., 2016. Combined effects of organic aerosol loading and fog processing on organic aerosols oxidation, composition, and evolution. *Sci. Total Environ.* 573, 690–698. <https://doi.org/10.1016/j.scitotenv.2016.08.156>.
- Chakraborty, A., Mandariya, A.K., Chakraborti, R., Gupta, T., Tripathi, S.N., 2018. Realtime chemical characterization of post monsoon organic aerosols in a

- polluted urban city: sources, composition, and comparison with other seasons. Environ. Pollut. 232. <https://doi.org/10.1016/j.envpol.2017.09.079>.
- Chang, R.Y.-W., Slowik, J.G., Shantz, N.C., Vlasenko, A., Liggio, J., Sjostedt, S.J., Leaitch, W.R., Abbatt, J.P.D., 2010. The hygroscopicity parameter (κ) of ambient organic aerosol at a field site subject to biogenic and anthropogenic influences: relationship. Atmos. Chem. Phys. 10, 5047–5064. <https://doi.org/10.5194/acp-10-5047-2010>.
- Charlson, R.J., Horvath, H., Pueschel, R.F., 1967. The direct measurement of atmospheric light scattering coefficient for studies of visibility and pollution. Atmospheric Environment 1 (4), 469–478. [https://doi.org/10.1016/0004-6981\(67\)90062-5](https://doi.org/10.1016/0004-6981(67)90062-5). In this issue.
- Chen, J., Budisulistiorini, S.H., Miyakawa, T., Komazaki, Y., Kuwata, M., 2018a. Secondary aerosol formation promotes water uptake by organic-rich wildfire haze particles in equatorial Asia. Atmos. Chem. Phys. 18, 7781–7798. <https://doi.org/10.5194/acp-18-7781-2018>.
- Chen, Y., Wild, O., Wang, Y., Ran, L., Teich, M., Größ, J., Wang, L., Spindler, G., Herrmann, H., van Pinxteren, D., McMinn, G., Wiedensohler, A., 2018b. The influence of impactor size cut-off shift caused by hygroscopic growth on particulate matter loading and composition measurements. Atmos. Environ. 195, 141–148. <https://doi.org/10.1016/j.atmosenv.2018.09.049>.
- Chowdhury, S., Dey, S., Smith, K.R., 2018. Ambient PM_{2.5} exposure and expected premature mortality to 2100 in India under climate change scenarios. Nat. Commun. 9. <https://doi.org/10.1038/s41467-017-02755-y>.
- Cusworth, D.H., Mickley, L.J., Sulprizio, M.P., Liu, T., Marlier, M.E., DeFries, R.S., Guttikunda, S.K., Gupta, P., 2018. Quantifying the influence of agricultural fires in northwest India on urban air pollution in Delhi, India. Environmental Research Letters 13 (4), 44018. <https://doi.org/10.1088/1748-9326/aab303>.
- Dandona, L., Dandona, R., Kumar, G.A., Shukla, D.K., Paul, V.K., Balakrishnan, K., Prabhakaran, D., Tandon, N., Salvi, S., Dash, A.P., Nandakumar, A., Patel, V., Agarwal, S.K., Gupta, P.C., Dhaliwal, R.S., Mathur, P., Laxmaiah, A., Dhillon, P.K., Dey, S., Mathur, M.R., Afshin, A., Fitzmaurice, C., Gakidou, E., Gething, P., Hay, S. I., Kassebaum, N.J., Kyu, H., Lim, S.S., Naghavi, M., Roth, G.A., Stanaway, J.D., Whiteford, H., Chada, V.K., Khaparde, S.D., Rao, R., Rade, K., Dewan, P., Furtado, M., Dutta, E., Varghese, C.M., Mehrotra, R., Jambulingam, P., Kaur, T., Sharma, M., Singh, S., Arora, R., Rasaily, R., Anjana, R.M., Mohan, V., Agrawal, A., Chopra, A., Mathew, A.J., Bhardwaj, D., Muraleedharan, P., Mutreja, P., Bienhoff, K., Glenn, S., Abdulkader, R.S., Aggarwal, A.N., Aggarwal, R., Albert, S., Ambekar, A., Arora, M., Bachani, D., Bavdekar, A., Beig, G., Bhangali, A., Bhargava, A., Bhatia, E., Camara, B., Christopher, D.J., Das, S.K., Dave, P.V., Dey, S., Ghoshal, A.G., Gopalakrishnan, N., Guleria, R., Gupta, R., Gupta, S.S., Gupta, T., Gupte, M.D., Gururaj, G., Harikrishnan, S., Iyer, V., Jain, S.K., Jeemon, P., Joshua, V., Kant, R., Kar, A., Kataki, A.C., Katoch, K., Khanna, T., Khera, A., Kinra, S., Koul, P.A., Krishnan, A., Kumar, A., Kumar, R.K., Kumar, R., Kurpad, A., Ladusingh, L., Lodha, R., Mahesh, P.A., Malhotra, R., Mathai, M., Mavalankar, D., Mohan, B.V., Mukhopadhyay, S., Murhekar, M., Murthy, G.V.S., Nair, S., Nair, S.A., Nanda, L., Nonnagaitthem, R.S., Oomen, A.M., Pandian, J.D., Pandya, S., Parameswaran, S., Pati, S., Prasad, K., Prasad, N., Purwar, M., Rahim, A., Raju, S., Ramji, S., Rangaswamy, T., Rath, G.K., Roy, A., Sabde, Y., Sachdeva, K.S., Sadhu, H., Sagar, R., Sankar, M.J., Sharma, R., Shet, A., Shirude, S., Shukla, R., Shukla, S.R., Singh, G., Singh, N.P., Singh, V., Sinha, A., Sinha, D.N., Srivastava, R.K., Srivaidya, A., Suri, V., Swaminathan, R., Sylaja, P. N., Tandale, B., Thakur, J.S., Thankappan, K.R., Thomas, N., Tripathy, S., Varghese, M., Varughese, S., Venkatesh, S., Venugopal, K., Vijayakumar, L., Xavier, D., Yajnik, C.S., Zachariah, G., Zodpey, S., Rao, J.V.R.P., Vos, T., Reddy, K.S., Murray, C.J.L., Swaminathan, S., 2017. Nations within a nation: variations in epidemiological transition across the states of India, 1990–2016 in the Global Burden of Disease Study. Lancet 390, 2437–2460. [https://doi.org/10.1016/S0140-6736\(17\)32804-0](https://doi.org/10.1016/S0140-6736(17)32804-0).
- DeCarlo, P.F., Kimmel, J.R., Trimborn, A., Northway, M.J., Jayne, J.T., Aiken, A.C., Gonin, M., Fuhrer, K., Horvath, T., Docherty, K.S., Worsnop, D.R., Jimenez, J.L., 2006. Field-deployable, high-resolution, time-of-flight aerosol mass spectrometer. Anal. Chem. 78, 8281–8289. <https://doi.org/10.1021/ac061249n>.
- DeCarlo, P.F., Slowik, J.G., Worsnop, D.R., Davidovits, P., Jimenez, J.L., 2004. Particle morphology and density characterization by combined mobility and aerodynamic diameter measurements. Part 1: Theory. Aerosol Sci. Technol. 38, 1185–1205. <https://doi.org/10.1080/027868290903907>.
- Deng, X., Tie, X., Wu, D., Zhou, X., Bi, X., Tan, H., Li, F., Jiang, C., 2008. Long-term trend of visibility and its characterizations in the Pearl River Delta (PRD) region. China. Atmos. Environ. 42, 1424–1435. <https://doi.org/10.1016/j.atmosenv.2007.11.025>.
- Duplissy, J., De Carlo, P.F., Dommen, J., Alfara, M.R., Metzger, A., Barmpadimos, I., Prevot, A.S.H., Weingartner, E., Tritscher, T., Gysel, M., Aiken, A.C., Jimenez, J.L., Canagaratna, M.R., Worsnop, D.R., Collins, D.R., Tomlinson, J., Baltensperger, U., 2011. Relating hygroscopicity and composition of organic aerosol particulate matter. Atmos. Chem. Phys. 11, 1155–1165. <https://doi.org/10.5194/acp-11-1155-2011>.
- Enroth, J., Mikkilä, J., Németh, Z., Kulmala, M., Salma, I., 2018. Wintertime hygroscopicity and volatility of ambient urban aerosol particles. Atmos. Chem. Phys. 18, 4533–4548. <https://doi.org/10.5194/acp-18-4533-2018>.
- Draxler, R., and G. D. Rolph (2003), HYSPLIT (HYbrid Single-Particle Lagrangian Integrated Trajectory) model, access via NOAA ARL READY Website (<http://www.arl.noaa.gov/ready/hysplit4.html>), NOAA Air Resources Lab., Silver Spring, Md.
- Fan, X., Zhang, F., Chen, L., Collins, D., Xu, W., Jin, X., Ren, J., Wang, Y., Wu, H., Li, S., Sun, Y., Li, Z., 2019. Contrasting ambient fine particles hygroscopicity derived by HTDMA and HR-AMS measurements between summer and winter in urban Beijing. Atmos. Chem. Phys. Discuss. 210, 1–30. <https://doi.org/10.5194/acp-2019-583>.
- Fountoukis, C., Nenes, A., 2007. ISORROPIA II: a computationally efficient thermodynamic equilibrium model for $K^+ - Ca^{2+} - Mg^{2+} - NH_4^+ - Na^+ - SO_4^{2-} - NO_3^- - Cl^- - H_2O$ aerosols. Atmos. Chem. Phys. 7, 4639–4659. <https://doi.org/10.5194/acp-7-4639-2007>.
- Gupta, T., Mandariya, A., 2013. Sources of submicron aerosol during fog-dominated wintertime at Kanpur. Environ. Sci. Pollut. Res. 20, 5615–5629. <https://doi.org/10.1007/s11356-013-1580-6>.
- Gysel, M., Crosier, J., Topping, D.O., Whitehead, J.D., Bower, K.N., Cubison, M.J., Williams, P.I., Flynn, M.J., McMinn, G.B., Coe, H., 2007. Closure study between chemical composition and hygroscopic growth of aerosol particles during TORCH2. Atmos. Chem. Phys. 7, 6131–6144. <https://doi.org/10.5194/acp-7-6131-2007>.
- Gysel, M., McMinn, G.B., Coe, H., 2009. Inversion of tandem differential mobility analyser (TDMA) measurements. J. Aerosol Sci. 40, 134–151. <https://doi.org/10.1016/j.jaerosci.2008.07.013>.
- Hong, J., Häkkinen, S.A.K., Paramonov, M., Äijälä, M., Hakala, J., Nieminen, T., Mikkilä, J., Prisle, N.L., Kulmala, M., Riipinen, I., Bilde, M., Kerminen, V.M., Petäjä, T., 2014. Hygroscopicity, CCN and volatility properties of submicron atmospheric aerosol in a boreal forest environment during the summer of 2010. Atmos. Chem. Phys. 14, 4733–4748. <https://doi.org/10.5194/acp-14-4733-2014>.
- Hong, J., Kim, J., Nieminen, T., Duplissy, J., Ehn, M., Äijälä, M., Hao, L.Q., Nie, W., Sarnela, N., Prisle, N.L., Kulmala, M., Virtanen, A., Petäjä, T., Kerminen, V.M., 2015. Relating the hygroscopic properties of submicron aerosol to both gas- and particle-phase chemical composition in a boreal forest environment. Atmos. Chem. Phys. 15, 11999–12009. <https://doi.org/10.5194/acp-15-11999-2015>.
- Hong, J., Xu, H., Tan, H., Yin, C., Hao, L., Li, F., Cai, M., Deng, X., Wang, N., Su, H., Cheng, Y., Wang, L., Petäjä, T., Kerminen, V.M., 2018. Mixing state and particle hygroscopicity of organic-dominated aerosols over the Pearl River Delta region in China. Atmos. Chem. Phys. 18, 14079–14094. <https://doi.org/10.5194/acp-18-14079-2018>.
- Jayne, J.T., Leard, D.C., Zhang, X., Davidovits, P., Smith, K.A., Kolb, C.E., Worsnop, D.R., 2000. Development of an aerosol mass spectrometer for size and composition analysis of submicron particles. Aerosol Sci. Technol. 33, 49–70. <https://doi.org/10.1080/027868200410840>.
- Jimenez, J.L., Jayne, J.T., Shi, Q., Kolb, C.E., Worsnop, D.R., Yourshaw, I., Seinfeld, J.H., Flagan, R.C., Zhang, X., Smith, K.A., Morris, J.W., Davidovits, P., 2003. Ambient aerosol sampling using the Aerodyne Aerosol Mass Spectrometer. J. Geophys. Res. 108, 8425. <https://doi.org/10.1029/2001JD001213>.
- Kanawade, V.P., Tripathi, S.N., Bhattu, D., Shamjad, P.M., 2014. Sub-micron particle number size distributions characteristics at an urban location, Kanpur, in the Indo-Gangetic Plain. Atmos. Res. 147–148, 121–132. <https://doi.org/10.1016/j.atmosres.2014.05.010>.
- Karanasiou, A., Amato, F., Moreno, T., Lumbreiras, J., Borge, R., Linares, C., Boldo, E., Alastuey, A., Querol, X., 2014. Road dust emission sources and assessment of street washing effect. Aerosol Air Qual. Res. 14, 734–743. <https://doi.org/10.4209/aaqr.2013.03.0074>.
- Kawana, K., Nakayama, T., Kubota, N., Mochida, M., 2017. Hygroscopicity and cloud condensation nucleus activity of forest aerosol particles during summer in Wakayama, Japan. J. Geophys. Res. 122, 3042–3064. <https://doi.org/10.1002/2016JD025660>.
- Kawana, K., Nakayama, T., Mochida, M., 2016. Hygroscopicity and CCN activity of atmospheric aerosol particles and their relation to organics: Characteristics of urban aerosols in Nagoya, Japan. J. Geophys. Res. Atmos. 121, 4100–4121. <https://doi.org/10.1002/2015JD023213>.
- Koehler, K.A., Kreidenweis, S.M., DeMott, P.J., Petters, M.D., Prenni, A.J., Carrico, C.M., 2009. Hygroscopicity and cloud droplet activation of mineral dust aerosol. Geophys. Res. Lett. 36, 1–5. <https://doi.org/10.1029/2009GL037348>.
- Kuwata, M., Zorn, S.R., Martin, S.T., 2012. Using elemental ratios to predict the density of organic material composed of carbon, hydrogen, and oxygen. Environ. Sci. Technol. 46, 787–794. <https://doi.org/10.1021/es202525q>.
- Li, X., Song, S., Zhou, W., Hao, J., Worsnop, D.R., Jiang, J., 2019. Interactions between aerosol organic components and liquid water content during haze episodes in Beijing 1–19.
- Mandariya, A.K., Gupta, T., Tripathi, S.N., 2019. Effect of aqueous-phase processing on the formation and evolution of organic aerosol (OA) under different stages of fog life cycles. Atmos. Environ. 206, 60–71. <https://doi.org/10.1016/j.atmosenv.2019.02.047>.
- Massoli, P., Lambe, A.T., Ahern, A.T., Williams, L.R., Ehn, M., Mikkilä, J., Canagaratna, M.R., Brune, W.H., Onasch, T.B., Jayne, J.T., Petäjä, T., Kulmala, M., Laaksonen, A., Kolb, C.E., Davidovits, P., Worsnop, D.R., 2010. Relationship between aerosol oxidation level and hygroscopic properties of laboratory generated secondary organic aerosol (SOA) particles. Geophys. Res. Lett. 37, 1–5. <https://doi.org/10.1029/2010GL045258>.
- Mei, F., Setyan, A., Zhang, Q., Wang, J., 2013. CCN activity of organic aerosols observed downwind of urban emissions during CARES. Atmos. Chem. Phys. 13, 12155–12169. <https://doi.org/10.5194/acp-13-12155-2013>.
- Mishra, G., Mandariya, A.K., Tripathi, S.N., Mariam, Joshi, Khan, A., Sapra, B.K., 2019. Hygroscopic growth of CsI and CsOH particles in context of nuclear reactor accident research. J. Aerosol Sci. 132, 60–69. <https://doi.org/10.1016/j.jaerosci.2019.03.008>.
- Nair, V.S., Moorthy, K.K., Alappattu, D.P., Kunhikrishnan, P.K., George, S., Nair, P.R., Babu, S.S., Abish, B., Satheesh, S.K., Tripathi, S.N., Niranjana, K., Madhavan, B.L., Srikanth, V., Dutt, C.B.S., Badarinath, K.V.S., Reddy, R.R., 2007. Wintertime aerosol characteristics over the Indo-Gangetic Plain (IGP): impacts of local boundary layer processes and long-range transport. J. Geophys. Res. Atmos. 112, 1–15. <https://doi.org/10.1029/2006JD008099>.

- Ng, N.L., Canagaratna, M.R., Jimenez, J.L., Chhabra, P.S., Seinfeld, J.H., Worsnop, D.R., 2011a. Changes in organic aerosol composition with aging inferred from aerosol mass spectra. *Atmos. Chem. Phys.* 11, 6465–6474. <https://doi.org/10.5194/acp-11-6465-2011>.
- Ng, N.L., Canagaratna, M.R., Jimenez, J.L., Zhang, Q., Ulbrich, I.M., Worsnop, D.R., 2011b. Real-time methods for estimating organic component mass concentrations from aerosol mass spectrometer data. *Environ. Sci. Technol.* 45, 910–916. <https://doi.org/10.1021/es102951k>.
- Ng, N.L., Canagaratna, M.R., Zhang, Q., Jimenez, J.L., Tian, J., Ulbrich, I.M., Kroll, J.H., Docherty, K.S., Chhabra, P.S., Bahreini, R., Murphy, S.M., Seinfeld, J.H., Hildebrandt, L., Donahue, N.M., Decarlo, P.F., Lanz, V.A., Prévôt, A.S.H., Dinar, E., Rudich, Y., Worsnop, D.R., 2010. Organic aerosol components observed in Northern Hemispheric datasets from Aerosol Mass Spectrometry. *Atmos. Chem. Phys.* 10, 4625–4641. <https://doi.org/10.5194/acp-10-4625-2010>.
- Ogawa, S., Setoguchi, Y., Kawana, K., Nakayama, T., Ikeda, Y., Sawada, Y., Matsumi, Y., Mochida, M., 2016. Hygroscopicity of aerosol particles and CCN activity of nearly hydrophobic particles in the urban atmosphere over Japan during summer. *J. Geophys. Res.* 121, 7215–7234. <https://doi.org/10.1002/2015JD024636>.
- Patidar, V., Tripathi, S.N., Bharti, P.K., Gupta, T., 2012. First surface measurement of cloud condensation nuclei over Kanpur, IGP: role of long range transport. *Aerosol Sci. Technol.* 46, 973–982. <https://doi.org/10.1080/02786826.2012.685113>.
- Petit, J.E., Favez, O., Albinet, A., Canonaco, F., 2017. A user-friendly tool for comprehensive evaluation of the geographical origins of atmospheric pollution: wind and trajectory analyses. *Environ. Model. Softw.* 88, 183–187. <https://doi.org/10.1016/j.envsoft.2016.11.022>.
- Petters, M.D., Kreidenweis, S.M., 2007. A single parameter representation of hygroscopic growth and cloud condensation nucleus activity. *Atmos. Chem. Phys.* 7, 1961–1971. <https://doi.org/10.5194/acp-7-1961-2007>.
- Rai, P., Chakraborty, A., Mandariya, A.K., Gupta, T., 2016. Composition and source apportionment of PM₁ at urban site Kanpur in India using PMF coupled with CBPF. *Atmos. Res.* 178–179, 506–520. <https://doi.org/10.1016/j.atmosres.2016.04.015>.
- Rajput, P., Mandariya, A., Kachawa, L., Singh, D.K., Singh, A.K., Gupta, T., 2016. Chemical characterisation and source apportionment of PM₁ during massive loading at an urban location in Indo-Gangetic Plain: impact of local sources and long-range transport. *Tellus, Ser. B Chem. Phys. Meteorol.* 68. <https://doi.org/10.3402/tellusb.v68.30659>.
- Rajput, P., Mandariya, A.K., Kachawa, L., Singh, D.K., Singh, A.K., Gupta, T., 2015. Wintertime source-apportionment of PM₁ from Kanpur in the Indo-Gangetic plain. *Clim. Chang.* 14, 503–507.
- Ram, K., Tripathi, S.N., Sarin, M.M., Bhattu, D., 2014. Primary and secondary aerosols from an urban site (Kanpur) in the Indo-Gangetic Plain: Impact on CCN, CN concentrations and optical properties. *Atmos. Environ.* 89, 655–663. <https://doi.org/10.1016/j.atmosenv.2014.02.009>.
- Randall, D.A., Wood, R.A., Bony, S., Colman, R., Fichefet, T., Fyfe, J., Kattsov, V., Pitman, A., Shukla, J., Srinivasan, J., Stouffer, R.J., Sumi, A., Taylor, K.E., 2007. Climate models and their evaluation. *Climate Change 2007 The Physical Science Basis*, .. Chapter 8. Cambridge Univ. Press, United Kingdom, pp. 589–662. United Kingdom: N. p. 2007. Web.
- Rissler, J., Nordin, E.Z., Eriksson, A.C., Nilsson, P.T., Frosch, M., Sporre, M.K., Wierzbicka, A., Svenssonsson, B., Löndahl, J., Messing, M.E., Sjogren, S., Hemmingsen, J.G., Loft, S., Pagels, J.H., Swietlicki, E., 2014a. Effective density and mixing state of aerosol particles in a near-traffic urban environment. *Environ. Sci. Technol.* 48, 6300–6308. <https://doi.org/10.1021/es5000353>.
- Rissler, J., Pagels, J., Swietlicki, E., Wierzbicka, A., Strand, M., Lillieblad, L., Sanati, M., Bohgard, M., 2014b. Hygroscopic behavior of aerosol particles emitted from biomass fired grate boilers. *Aerosol Sci. Technol.* 39, 919–930. <https://doi.org/10.1080/02786820500331068>.
- Roy, A., Chatterjee, A., Sarkar, C., Das, S.K., Ghosh, S.K., Raha, S., 2017. A study on aerosol-cloud condensation nuclei (CCN) activation over eastern Himalaya in India. *Atmospheric Research* 189, 69–81. <https://doi.org/10.1016/j.atmosres.2017.01.015>.
- Seinfeld, J.H., Pandis, S.N., 2006. *Atmospheric Chemistry and Physics: From Air Pollution to Climate Change*. John Wiley & Sons Inc.
- Shamjad, P.M., Tripathi, S.N., Pathak, R., Hallquist, M., Arola, A., Bergin, M.H., 2015. Contribution of brown carbon to direct radiative forcing over the Indo-Gangetic plain. *Environ. Sci. Technol.* 49, 10474–10481. <https://doi.org/10.1021/acs.est.5b03368>.
- Singh, D.K., Gupta, T., 2016. Effect through inhalation on human health of PM₁ bound polycyclic aromatic hydrocarbons collected from foggy days in northern part of India. *J. Hazard. Mater.* 306, 257–268. <https://doi.org/10.1016/j.jhazmat.2015.11.049>.
- Sjogren, S., Gysel, M., Weingartner, E., Alfara, M.R., Duplissy, J., Cozic, J., Crosier, J., Coe, and U.B., 2012. Hygroscopicity of the submicrometer aerosol at the high-alpine site Jungfraujoch, 3580m a.s.l., Switzerland 7231–7249. doi: 10.5194/acp-12-7231-2012.
- Sjogren, S., Gysel, M., Weingartner, E., Baltensperger, U., Cubison, M.J., Coe, H., Zardini, A.A., Marcolla, C., Krieger, U.K., Peter, T., 2007. Hygroscopic growth and water uptake kinetics of two-phase aerosol particles consisting of ammonium sulfate, adipic and humic acid mixtures. *J. Aerosol Sci.* 38, 157–171. <https://doi.org/10.1016/j.jaerosci.2006.11.005>.
- Sun, Y., Wang, Z., Fu, P., Jiang, Q., Yang, T., Li, J., Ge, X., 2013. The impact of relative humidity on aerosol composition and evolution processes during wintertime in Beijing, China. *Atmospheric Environment* 77, 927–934. <https://doi.org/10.1016/j.atmosenv.2013.06.019>.
- Tang, I.N., Munkelwitz, H.R., 1994. Water activities, densities, and refractive indices of aqueous sulfates and sodium nitrate droplets of atmospheric importance. *J. Geophys. Res.* <https://doi.org/10.1029/94JD01345>.
- Topping, D.O., McFiggans, G.B., Coe, H., 2005. A curved multi-component aerosol hygroscopicity model framework: Part 1 – Inorganic compounds. *Atmos. Chem. Phys.* 5, 1205–1222. <https://doi.org/10.5194/acp-5-1205-2005>.
- Tritscher, T., Dommen, J., DeCarlo, P.F., Gysel, M., Barmet, P.B., Praplan, A.P., Weingartner, E., Prévôt, A.S.H., Riipinen, I., Donahue, N.M., Baltensperger, U., 2011a. Volatility and hygroscopicity of aging secondary organic aerosol in a smog chamber. *Atmos. Chem. Phys.* 11, 11477–11496. <https://doi.org/10.5194/acp-11-11477-2011>.
- Tritscher, T., Jurányi, Z., Martin, M., Chirico, R., Gysel, M., Heringa, M.F., DeCarlo, P.F., Sierau, B., Prévôt, A.S.H., Weingartner, E., Baltensperger, U., 2011b. Changes of hygroscopicity and morphology during ageing of diesel soot. *Environ. Res. Lett.* 6. <https://doi.org/10.1088/1748-9326/6/3/034026> 034026.
- Villani, P., Picard, D., Michaud, V., Laj, P., Wiedensohler, A., 2008. Design and validation of a volatility hygroscopic Tandem Differential Mobility Analyzer (VH-TDMA) to characterize the relationships between the thermal and hygroscopic properties of atmospheric aerosol particles. *Aerosol Sci. Technol.* 42, 729–741. <https://doi.org/10.1080/02786820802255668>.
- Wang, X., Shen, X.J., Sun, J.Y., Zhang, X.Y., Wang, Y.Q., Zhang, Y.M., Wang, P., Xia, C., Qi, X.F., Zhong, J.T., 2018. Size-resolved hygroscopic behavior of atmospheric aerosols during heavy aerosol pollution episodes in Beijing in December 2016. *Atmos. Environ.* 194, 188–197. <https://doi.org/10.1016/j.atmosenv.2018.09.041>.
- Wang, Y., Chen, Y., 2019. Significant climate impact of highly hygroscopic atmospheric aerosols in Delhi, India. *Geophys. Res. Lett.* 2019GL082339. doi: 10.1029/2019GL082339.
- Wester, P., Mishra, A., Mukherji, A., Shrestha, A.B., Change, C., 2019. The Hindu Kush Himalaya Assessment, The Hindu Kush Himalaya Assessment. <https://doi.org/10.1007/978-3-319-92288-1>.
- WMO/GAW: WMO/GAW Aerosol Measurement Procedures, Guidelines and Recommendations, GAW Report No. 227, available at: <https://library.wmo.int/> (last access: 18 September 2018). 2016.
- Wu, Z.J., Zheng, J., Shang, D.J., Du, Z.F., Wu, Y.S., Zeng, L.M., Wiedensohler, A., Hu, M., 2016. Particle hygroscopicity and its link to chemical composition in the urban atmosphere of Beijing, China, during summertime. *Atmos. Chem. Phys.* 16, 1123–1138. <https://doi.org/10.5194/acp-16-1123-2016>.
- Xu, W., Han, T., Du, W., Wang, Q., Chen, C., Zhao, J., Zhang, Y., Li, J., Fu, P., Wang, Z., Worsnop, D.R., Sun, Y., 2017. Effects of aqueous-phase and photochemical processing on secondary organic aerosol formation and evolution in Beijing, China. *Environ. Sci. Technol.* 51, 762–770. <https://doi.org/10.1021/acs.est.6b04498>.
- Yeung, M.C., Lee, B.P., Li, Y.J., Chan, C.K., 2014. Simultaneous HTDMA and HR-ToF-AMS measurements at the HKUST supersite in Hong Kong in 2011. *J. Geophys. Res.* 119, 9864–9883. <https://doi.org/10.1002/2013JD021146>.
- Zelenyuk, A., Cai, Y., Imre, D., 2006. From agglomerates of spheres to irregularly shaped particles: determination of dynamic shape factors from measurements of mobility and vacuum aerodynamic diameters. *Aerosol Sci. Technol.* 40, 197–217. <https://doi.org/10.1080/02786820500529406>.
- Zhang, Q., Alfara, M.R., Worsnop, D.R., James, D., Coe, H., Canagaratna, M.R., Jimenez, J.L., 2005. Deconvolution and quantification of hydrocarbon-like and oxygenated organic aerosols based on aerosol mass spectrometry deconvolution and quantification of hydrocarbon-like and oxygenated organic aerosols based on aerosol mass spectrometry. *Environ. Sci. Technol.* 39, 4938–4952. <https://doi.org/10.1021/es0485681>.
- Zhou, Y., Zhang, H., Parikh, H.M., Chen, E.H., Rattanavaraha, W., Rosen, E.P., Wang, W., Kamens, R.M., 2011. Secondary organic aerosol formation from xylenes and mixtures of toluene and xylenes in an atmospheric urban hydrocarbon mixture: water and particle seed effects (II). *Atmos. Environ.* 45, 3882–3890. <https://doi.org/10.1016/j.atmosenv.2010.12.048>.